CrossMark

J/M PAPERS

Weak nonlinearity for strong non-normality

Yves-Marie Ducimetière[1,†], **Edouard Boujo**[1] **and François Gallaire**[1]

[1]Laboratory of Fluid Mechanics and Instabilities, EPFL, CH1015 Lausanne, Switzerland

We propose a theoretical approach to derive amplitude equations governing the weakly nonlinear evolution of non-normal dynamical systems, when they experience transient growth or respond to harmonic forcing. This approach reconciles the non-modal nature of these growth mechanisms and the need for a centre manifold to project the leading-order dynamics. Under the hypothesis of strong non-normality, we take advantage of the fact that small operator perturbations suffice to make the inverse resolvent and the inverse propagator singular, which we encompass in a multiple-scale asymptotic expansion. The methodology is outlined for a generic nonlinear dynamical system, and four application cases highlight common non-normal mechanisms in hydrodynamics: the streamwise convective non-normal amplification in the flow past a backward-facing step, and the Orr and lift-up mechanisms in the plane Poiseuille flow.

Key words: nonlinear dynamical systems, instability

1. Introduction

Nonlinear dynamical systems can have one or several equilibrium solutions, which form one of the building blocks of the phase space (Strogatz 2015). The linear stability of an equilibrium can be deduced from the eigenvalues of the linearised operator: linear modal analysis thus helps to detect bifurcations and distinguish between linearly unstable, neutral (marginally stable) and strictly stable equilibria, when the largest growth rate is positive, null and negative, respectively. The linear modal analysis sometimes remains too simplistic, however, and has therefore been generalised over the last decades to account for nonlinear (Stuart 1960) and non-modal (Trefethen *et al.* 1993) effects, although these two types of correction have generally been opposed, culminating in F. Waleffe's paper entitled 'Nonlinear normality vs non-normal linearity' (Waleffe 1995). The objective of the present

947 A43-1

study is precisely to contribute to reconciling nonlinearity and non-normality, and to rigorously deriving weakly nonlinear amplitude equations ruling non-normal systems.

1.1. *Strong non-normality*

Upon the choice of a scalar product, a linear operator is non-normal if it does not commute with its adjoint. Consequently, its eigenmodes do not form an orthogonal set, and the response to an initial condition or to time-harmonic forcing may be highly non-trivial (see Trefethen & Embree (2005) for an exhaustive presentation). This response generally results from an intricate cooperation between a large number of eigenmodes. The leading (least stable or most unstable) eigenvalue solely provides the asymptotic (long-time) linear behaviour of the energy of the unforced system. At finite time, restriction to the leading eigenmode is generally irrelevant. In particular, a negative growth rate for all eigenvalues is not a guarantee for the energy to decay monotonically for all initial conditions: some small-amplitude perturbations may experience a large transient amplification (figure 1*a*). The same is true for systems subject to harmonic forcing: they may exhibit strong amplification, much larger than the inverse of the smallest damping rate, and at forcing frequencies unpredictable at the sight of the spectrum (figure 1*b*).

Non-normal operators are encountered in various fields. In laser physics (see Trefethen & Embree 2005, § 60), H.J. Landau described non-normality by developing the concept of the pseudospectrum, as a pertinent alternative to modal analysis (Landau 1976, 1977). Non-normality in an unstable laser cavity results in a substantial increase in the linewidth of the laser beam signal compared with a perfect resonator (Petermann 1979). In astrophysics, Jaramillo, Macedo & Sheikh (2021) recently used a pseudospectrum analysis to study the stability of black holes. In network science, Asllani, Lambiotte & Carletti (2018) have shown that many directed empirical networks in various disciplines (biology, sociology, communication, transport, etc.) present strong non-normality. For instance, the non-normality of the London Tube network can result in the outbreak of a measles epidemic, although linear stability theory predicts an asymptotic decay of the number of contagions.

In hydrodynamics, non-normality is frequent and inherited from the linearisation of the advective term $(U \cdot \nabla)U$, U being the velocity field of the fluid flow. This term gives a preferential direction to the fluid flow, which breaks the normality of the linear operator. In the context of parallel flows, non-normality is found for instance in the canonical plane Couette and Poiseuille flows (Gustavsson 1991; Butler & Farrell 1992; Farrell & Ioannou 1993; Reddy & Henningson 1993; Schmid & Henningson 2001), in pipe flow (Schmid & Henningson 1994) and in boundary layers (Butler & Farrell 1992; Corbett & Bottaro 2000). Non-normality is also found in non-parallel flows (Cossu & Chomaz 1997), for instance spatially developing boundary layers (Ehrenstein & Gallaire 2005; Åkervik *et al.* 2008; Monokrousos *et al.* 2010), jets (Garnaud *et al.* 2013*a,b*) and the flow past a backward-facing step (Blackburn, Barkley & Sherwin 2008; Boujo & Gallaire 2015). Exhaustive reviews of non-normality in hydrodynamics can be found in Chomaz (2005) and Schmid (2007). The crucial role played by non-normality in the transition to turbulence has become clear over the years (Trefethen *et al.* 1993; Baggett & Trefethen 1997; Schmid 2007). If the flow is non-normal, low-energy perturbations such as free-stream turbulence or wall roughness can be amplified strongly enough to lead to a regime where nonlinearities come into play, which may lead to turbulence through a sub-critical bifurcation. The toy system presented in Trefethen *et al.* (1993) is an excellent illustration of this so-called 'bypass' scenario.
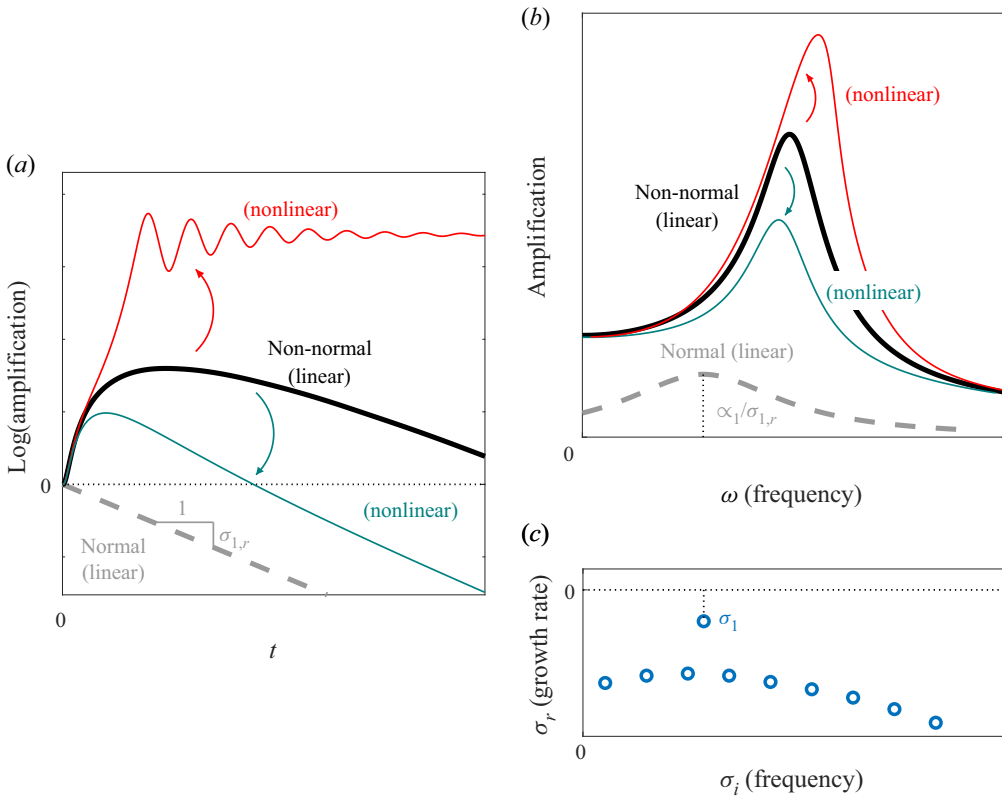
Figure 1. Cartoon representation of nonlinearity and non-normality, illustrated in the time domain (*a*) and frequency domain (*b*), for a linearly stable system; the least stable eigenvalue σ_1 of the eigenspectrum in (*c*) has indeed a negative growth rate. (*a*) In the linear regime, the amplitude of the perturbations eventually decays like $\exp(\sigma_{1,r}t)$. Non-normal systems can experience a very large transient growth. Nonlinearity may be stabilising or destabilising. (*b*) Normal systems subject to external forcing respond preferentially at frequency $\sigma_{1,i}$. Non-normal systems can respond at different frequencies, with an amplification much larger than predicted by $\sigma_{1,r}$. Nonlinearity may be stabilising or destabilising.

1.2. *Weak nonlinearity*

This illustrates the importance of combining nonlinearity and non-normality. In the bypass transition scenario, it is the conjunction of non-normality and nonlinearity which succeeds in shrinking the basin of attraction of a linearly strictly stable equilibrium, as strong amplification triggers nonlinearities (figure 1), and may radically change the behaviour of dynamical systems. Weakly or fully nonlinear effects can be introduced in the analysis. Notwithstanding the relevance and usefulness of fully nonlinear solutions (Hof *et al.* 2004; Schneider, Gibson & Burke 2010), as well as the existence of a fully nonlinear non-normal stability theory able to compute nonlinear optimal initial conditions via Lagrangian optimisation (Cherubini *et al.* 2010, 2011; Pringle & Kerswell 2010; Kerswell 2018), we believe that establishing a rigorous reduced-order model for weak nonlinearities is relevant. To the best of our knowledge, weakly nonlinear approaches all hinge on the fact that an amplitude equation can only be constructed close to a bifurcation point. Indeed, only linearised systems with a neutral or weakly damped eigenmode may experience resonance, whose avoidance condition results in the amplitude equation.

Following the insight of L. Landau, who introduced amplitude equations in analogy to phase transitions (Landau & Lifshitz 1987, § 26), weakly nonlinear analyses using a multiple-scale approach were performed in some pioneering works in the context of thermal convection (Gor'kov 1957; Malkus & Veronis 1958), parallel shear flows (Stuart 1958, 1960; Watson 1960) and non-parallel shear flows (Sipp & Lebedev 2007). In these studies, a so-called Stuart–Landau equation of the form $d_T A = \lambda A - \kappa A |A|^2$ is obtained for the bifurcated mode amplitude A as a condition for non-resonance. When the real part of the nonlinear coefficient is strictly positive, $\text{Re}(\kappa) > 0$, the cubic term $A|A|^2$ is sufficient to capture the saturation amplitude, and the Stuart–Landau equation is an accurate model for supercritical bifurcations; otherwise it can be extended to describe subcritical bifurcations as well.

Amplitude equations can be generalised to describe slow dependence on space (see Cross & Hohenberg (1993) for a review) and are also widely used to describe spatio-temporal pattern formation in physical systems near the bifurcation threshold. Beyond hydrodynamics, this occurs in plasma physics, solidification fronts, nonlinear optics, laser physics, oscillatory chemical reactions, buckling of elastic rods and many other fields.

While the form of the amplitude equation can often be deduced from symmetry considerations (Crawford & Knobloch 1991; Fauve 1998), its coefficients (λ and κ in the case of the Stuart–Landau equation) are evaluated with scalar products of fields computed at the bifurcation point. Other approaches exist to deduce the normal form, i.e. the amplitude equation which distillates the quintessence of the nonlinear behaviour in the vicinity of a bifurcation point (Guckenheimer & Holmes 1983; Manneville 2004; Haragus & Iooss 2011). Common to all these approaches is the concept of the centre manifold, along which the dynamics is slow, while, under a spectral gap assumption, an adiabatic elimination ensures the slaving of quickly damped modes.

1.3. *Amplitude equations without eigenvalues*

It is now understood that the application of asymptotic approaches to describe the weakly nonlinear behaviour of non-normal systems is not straightforward, because of the absence of a neutral bifurcation point in many non-normal systems. Note that, even when a system has a neutral or weakly damped mode, it can still exhibit large non-normality, which could jeopardise the relevance of a classical, single-mode amplitude equation.

The present work proposes to reconcile amplitude equations and non-normality. Specifically, a method is advanced to derive amplitude equations in the context of (i) harmonic forcing and (ii) transient growth. In case (i), we vary the amplitude of a given harmonic forcing at a prescribed frequency and predict the gain (energy growth) of the asymptotic response (§ 2). In case (ii), we vary the amplitude of a given initial condition and predict the gain of the response at a selected time $t = t_o$ (§ 3). In both cases, we perform an *a priori* weakly nonlinear prolongation of the gain, at very low numerical cost. The applied harmonic forcing and initial condition are allowed to be arbitrarily different from any eigenmode. The method does not rely on the presence of an eigenvalue close to the neutral axis; instead, it applies to any sufficiently non-normal operator. If such an eigenvalue is nevertheless present on the neutral axis, we recover a classical, modal amplitude equation. The method is illustrated with two flows, the non-parallel flow past a backward-facing step (sketched in figure 2*a*) and the parallel plane Poiseuille flow (figure 2*b*). These two non-normal flows exhibit large gains, both in the context of harmonic forcing (§§ 2.1–2.2) and transient growth (§§ 3.1–3.2).
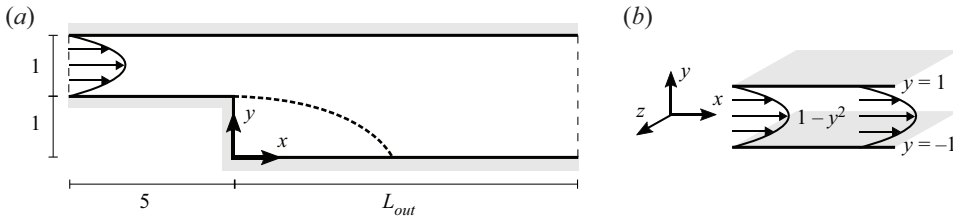
Figure 2. Sketch of the flow configurations. (*a*) Two-dimensional flow over a backward-facing step, with fully developed parabolic profile of unit maximum centreline velocity at the inlet. (*b*) Three-dimensional plane Poiseuille flow, confined between two solid walls at $y = \pm 1$, and invariant in the x (streamwise) and z (spanwise) directions.

In both contexts, a generic nonlinear dynamical system is considered

$$\partial_t U = N(U) + F, \quad U(0) = U_0, \tag{1.1}$$

where $N(*)$ is a nonlinear operator and F is a forcing term. An appropriate and common step to begin the analysis of (1.1) is to linearise it around an unforced equilibrium. The latter is denoted U_e and satisfies $N(U_e) = 0$. Around this equilibrium are considered small-amplitude perturbations in velocity ϵu, forcing ϵf and initial condition ϵu_0, where $\epsilon \ll 1$. An asymptotic expansion of (1.1) in terms of ϵ can thus be performed, transforming the nonlinear equation into a series of linear ones. The fields u, f and u_0 are recovered at order ϵ and linked through the linear relation

$$\partial_t u = Lu + f, \quad u(0) = u_0, \tag{1.2}$$

where L results from the linearisation of N around U_e. For fluid flows governed by the incompressible Navier–Stokes equations, $Lu = -(U_e \cdot \nabla)u - (u \cdot \nabla)U_e + Re^{-1}\Delta u - \nabla p(u)$, where the pressure field p is such that the velocity field u is divergence free. Both fields are linked through a linear Poisson equation. In practice, pressure is included in the state variable, resulting in a singular mass matrix; it is omitted here, for the sake of clarity.

2. Response to harmonic forcing

We first derive an amplitude equation for the weakly nonlinear amplification of time-harmonic forcing $f(x, t) = \hat{f}(x)e^{i\omega_o t} + \text{c.c.}$ (where c.c. is complex conjugate and ω_o designates the frequency) in a linearly strictly stable system. In the long-time regime, only the same-frequency harmonic response $u(x, t) = \hat{u}(x)e^{i\omega_o t} + \text{c.c.}$ persists. Injecting the expressions of f and u in (1.2) leads to $\hat{u} = (i\omega_o I - L)^{-1}\hat{f} \doteq R(i\omega_o)\hat{f}$, where $R(z) = (zI - L)^{-1}$ is the resolvent operator, and I is the identity operator. In the current context, it maps a harmonic forcing structure onto its asymptotic linear response at the same frequency. A measure of the maximum gain is

$$G(i\omega_o) = \max_{\hat{f}} \frac{\|\hat{u}\|}{\|\hat{f}\|} = \|R(i\omega_o)\| \doteq \frac{1}{\epsilon_o}. \tag{2.1}$$

In the following, we choose the L^2 norm (or 'energy' norm) induced by the Hermitian inner product $\langle \hat{u}_a, \hat{u}_b \rangle = \int_\Omega \hat{u}_a^H \hat{u}_b \, d\Omega$ (the superscript H denotes the Hermitian transpose). The operator $R(i\omega_o)^\dagger$ denotes the adjoint of $R(i\omega_o)$ under this scalar product, such that $\langle R(i\omega_o)\hat{u}_a, \hat{u}_b \rangle = \langle \hat{u}_a, R(i\omega_o)^\dagger \hat{u}_b \rangle$, for any $\hat{u}_a, \hat{u}_b$. Among all frequencies ω_o, the one leading to the maximum amplification is noted $\omega_{o,m}$ and associated with an optimal gain

$G(\mathrm{i}\omega_{o,m}) = 1/\epsilon_{o,m}$. The singular-value decomposition of $R(\mathrm{i}\omega_o)$ provides $G(\mathrm{i}\omega_o) = \epsilon_o^{-1}$ as the largest singular value, and the associated pair of right singular vector $\hat{\boldsymbol{f}}_o$ and left singular vector $\hat{\boldsymbol{u}}_o$. The former represents the optimal forcing, whereas the latter characterises the long-time-harmonic response reached, after the transients fade away

$$R(\mathrm{i}\omega_o)^{-1}\hat{\boldsymbol{u}}_o = \epsilon_o\hat{\boldsymbol{f}}_o, \quad \left[R(\mathrm{i}\omega_o)^{\dagger}\right]^{-1}\hat{\boldsymbol{f}}_o = \epsilon_o\hat{\boldsymbol{u}}_o, \tag{2.2}$$

where $\|\hat{\boldsymbol{f}}_o\| = \|\hat{\boldsymbol{u}}_o\| = 1$. Smaller singular values of $R(\mathrm{i}\omega_o)$ constitute sub-optimal gains, and the associated right singular vectors are sub-optimal forcing structures. Note that one can express $\langle \hat{\boldsymbol{u}}, \hat{\boldsymbol{u}} \rangle = \langle R\hat{\boldsymbol{f}}, R\hat{\boldsymbol{f}} \rangle$ as $\langle R^{\dagger}R\hat{\boldsymbol{f}}, \hat{\boldsymbol{f}} \rangle$, such that the singular values of $R(\mathrm{i}\omega_o)$ are also the square root of the eigenvalues of the symmetric operator $R(\mathrm{i}\omega_o)^{\dagger}R(\mathrm{i}\omega_o)$. An important implication is that the singular vectors form an orthogonal set for the scalar product $\langle *, * \rangle$. The practical computation of ϵ_o, $\hat{\boldsymbol{f}}_o$ and $\hat{\boldsymbol{u}}_o$ is detailed for the Navier–Stokes equations in Garnaud *et al.* (2013*b*), for instance. Note that, if the operator L possesses a neutral eigenvalue, $\omega_{o,m}, \hat{\boldsymbol{f}}_o$ and $\hat{\boldsymbol{u}}_o$ respectively reduce to the frequency, the adjoint and the direct mode associated with this eigenvalue.

Since L is strongly non-normal, as assumed in the rest of the present study, none of ϵ_o, $\hat{\boldsymbol{u}}_o$ and $\hat{\boldsymbol{f}}_o$ are immediately determined from its spectral (modal) properties. Strong non-normality implies $\epsilon_o \ll 1$, such that the inverse resolvent $R(\mathrm{i}\omega_o)^{-1}$ appearing in (2.2) is almost singular. We perturb it as

$$\Phi \doteq R(\mathrm{i}\omega_o)^{-1} - \epsilon_o P, \quad \text{with } P = \hat{\boldsymbol{f}}_o\langle \hat{\boldsymbol{u}}_o, * \rangle, \tag{2.3}$$

where the linear operator P is such that $P\hat{\boldsymbol{g}} = \hat{\boldsymbol{f}}_o\langle \hat{\boldsymbol{u}}_o, \hat{\boldsymbol{g}} \rangle$, for any field $\hat{\boldsymbol{g}}$ (note that $\langle \hat{\boldsymbol{u}}_o, * \rangle$ would write more simply '$\langle \hat{\boldsymbol{u}}_o|$' in the quantum mechanics formalism). This leads to $\Phi\hat{\boldsymbol{u}}_o = \boldsymbol{0}$, such that Φ is exactly singular. The norm of the perturbation operator is small since $\|P\| = 1$. The field $\hat{\boldsymbol{u}}_o$ constitutes the only non-trivial part of the kernel of Φ, and its associated adjoint mode is $\hat{\boldsymbol{f}}_o$. Indeed, using that $P^{\dagger} = \hat{\boldsymbol{u}}_o\langle \hat{\boldsymbol{f}}_o, * \rangle$, we have

$$\Phi^{\dagger}\hat{\boldsymbol{f}}_o = \left[R(\mathrm{i}\omega_o)^{-1}\right]^{\dagger}\hat{\boldsymbol{f}}_o - \epsilon_o\hat{\boldsymbol{u}}_o\langle \hat{\boldsymbol{f}}_o, \hat{\boldsymbol{f}}_o \rangle$$
$$= \left[R(\mathrm{i}\omega_o)^{\dagger}\right]^{-1}\hat{\boldsymbol{f}}_o - \epsilon_o\hat{\boldsymbol{u}}_o = \boldsymbol{0}, \tag{2.4}$$

where we used the fact that the inverse of the adjoint is the adjoint of the inverse. We note that Φ can be rewritten as $\Phi = (\mathrm{i}\omega_o I - L_n)$ where $L_n \doteq L + \epsilon_o P$, such that (2.3) seems to imply that the state operator L has been perturbed. In this process, the operator L_n has acquired an eigenvalue equal to $\mathrm{i}\omega_o$, and therefore has become neutral. However, it has also lost its reality and therefore does not, in general, possess an eigenvalue equal to $-\mathrm{i}\omega_o$. By construction, ϵ_o is the smallest possible amplitude of the right-hand side of (2.2) for a given $\mathrm{i}\omega_o$, such that $\epsilon_o P$ is the smallest perturbation of L necessary to relocate an eigenvalue of L on $\mathrm{i}\omega_o$. This fact can be formalised with the pseudospectrum theory outlined in Trefethen & Embree (2005). In the complex plane, $z \in \mathbb{C}$ belongs to the ϵ-pseudospectrum $\Lambda_\epsilon(L)$ if and only if $\|R(z)\| \geq 1/\epsilon$. If E is an operator with $\|E\| = 1$, eigenvalues of $L - \epsilon E$ can lie anywhere inside $\Lambda_\epsilon(L)$. Eigenvalues of L and singularities of $\|R(z)\|$ thus collide with the ϵ-pseudospectrum in the limit $\epsilon \to 0$. As ϵ increases, the ϵ-pseudospectrum may touch the imaginary axis, such that any $z = \mathrm{i}\omega_o$ can be an eigenvalue of $L - \epsilon E$ if the amplitude of the perturbation is greater than or equal to $\epsilon = \|R(\mathrm{i}\omega_o)\|^{-1}$. We recognise ϵ as the inverse
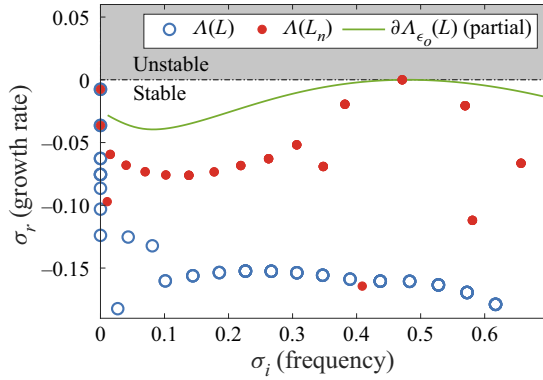
Figure 3. Natural and perturbed spectra of the flow past a backward-facing step (sketched in figure 2a) at Reynolds number $Re = 500$. Blue circles: eigenvalues of the linearised Navier–Stokes operator L. Red dots: eigenvalues of the linear operator perturbed with $\epsilon_o P = \epsilon_o \hat{\boldsymbol{f}}_o \langle \hat{\boldsymbol{u}}_o, * \rangle$. By construction, one eigenvalue of $L_n = L + \epsilon_o P$ lies on the imaginary axis. Green isocontour: part of the ϵ_o-pseudospectrum of L, where $\|R(z)\| = 1/\epsilon_o$. By construction, the ϵ_o-pseudospectrum is contained in the stable half-plane, except at $i\omega_o$ where it touches the neutral axis.

gain ϵ_o defined in (2.1), and thus E as P. In particular, if $\omega_o = \omega_{o,m}$, the associated $\epsilon_{o,m}$ is referred to as the stability radius of L since the $\epsilon_{o,m}$-pseudospectrum is the first to touch the imaginary axis.

As an illustration of the fact that a small-amplitude perturbation can easily 'neutralise' a non-normal operator, we consider the Navier–Stokes operator linearised around the steady flow past a backward-facing step (BFS), sketched in figure 2, at Reynolds number $Re = 500$. The most amplified frequency $\omega_o = \omega_{o,m} \approx 0.47$ is associated with $\epsilon_o \approx 1.3 \times 10^{-4} \ll 1$. The spectra of L and L_n are shown in figure 3, together with part of the ϵ_o-pseudospectrum of L. Clearly, the very small perturbation $\epsilon_o P$ locates an eigenvalue exactly onto $i\omega_o$, despite the strong stability of L. We stress that neither ω_o nor ϵ_o can be deduced only by inspecting the spectrum of L.

Nevertheless, in what follows, it is really the inverse resolvent and not the state operator L that we propose to perturb. Indeed, L is generally a real operator whereas L_n is necessarily a complex one, and only one side of the spectrum of L_n can generally be made neutral at a time, depending on whether L is perturbed with P or its complex conjugate P^*.

The inverse gain $\epsilon_o \ll 1$ constitutes a natural choice of small parameter. We choose the Navier–Stokes equations for their nonlinear term $(U \cdot \nabla)U$, which yields both a non-normal linearised operator and a rich diversity of behaviours. The flow is weakly forced by $\boldsymbol{F} = \phi \sqrt{\epsilon_o}^3 \hat{\boldsymbol{f}}_h e^{i\omega_o t} + \text{c.c.}$, where $\hat{\boldsymbol{f}}_h$ is an arbitrary (not necessarily optimal) forcing structure, and $\phi = O(1)$ is a real prefactor. Imposing $\|\hat{\boldsymbol{f}}_h\| = 1$, the forcing amplitude is $F \doteq \phi \sqrt{\epsilon_o}^3$. A separation of time scales is invoked for the flow response: its envelope is assumed to vary on a slow time scale $T = \epsilon_o t$ (such that $d_t = \partial_t + \epsilon_o \partial_T$). This ensures a comprehensive distinguished scaling and suggests the following multiple-scale expansion:

$$U(t, T) = U_e + \sqrt{\epsilon_o} \boldsymbol{u}_1(t, T) + \epsilon_o \boldsymbol{u}_2(t, T) + \sqrt{\epsilon_o}^3 \boldsymbol{u}_3(t, T) + O(\epsilon_o^2). \qquad (2.5)$$

The velocity field at each order j is then Fourier expanded as

$$\boldsymbol{u}_j(t, T) = \bar{\boldsymbol{u}}_{j,0}(T) + \sum_m (\bar{\boldsymbol{u}}_{j,m}(T) e^{im\omega_o t} + \text{c.c.}), \qquad (2.6)$$

with $m = 1, 2, 3 \ldots$. This decomposition is certainly justified in the permanent regime, of interest in this analysis. The proposed slow dynamics does not aim to capture the transient regime but flow variations around the permanent regime. Introducing (2.5)–(2.6) into the Navier–Stokes equations and using (2.3) to perturb the operator $R(i\omega_o)^{-1}$ appearing from time derivation yields

$$
\begin{aligned}
&\sqrt{\epsilon_o}\left[\left(\Phi\bar{\boldsymbol{u}}_{1,1}\mathrm{e}^{\mathrm{i}\omega_o t} + \text{c.c.}\right) + \boldsymbol{s}_1\right] + \epsilon_o\left[\left(\Phi\bar{\boldsymbol{u}}_{2,1}\mathrm{e}^{\mathrm{i}\omega_o t} + \text{c.c.}\right) + \boldsymbol{s}_2 + C(\boldsymbol{u}_1, \boldsymbol{u}_1)\right] \\
&\quad + \sqrt{\epsilon_o}^3\left[\left(\Phi\bar{\boldsymbol{u}}_{3,1}\mathrm{e}^{\mathrm{i}\omega_o t} + \text{c.c.}\right) + \boldsymbol{s}_3 + 2C(\boldsymbol{u}_1, \boldsymbol{u}_2) + \partial_T\boldsymbol{u}_1 + \left(P\bar{\boldsymbol{u}}_{1,1}\mathrm{e}^{\mathrm{i}\omega_o t} + \text{c.c.}\right)\right] + O(\epsilon_o^2) \\
&= \phi\sqrt{\epsilon_o}^3\hat{\boldsymbol{f}}_h\mathrm{e}^{\mathrm{i}\omega_o t} + \text{c.c.},
\end{aligned} \tag{2.7}
$$

where

$$
\boldsymbol{s}_j \doteq -L\bar{\boldsymbol{u}}_{j,0}(T) + \left[\sum_m(\mathrm{i}m\omega_o - L)\bar{\boldsymbol{u}}_{j,m}(T)\mathrm{e}^{\mathrm{i}m\omega_o t} + \text{c.c.}\right], \tag{2.8}
$$

for $m = 2, 3, \ldots$, and $C(\boldsymbol{a}, \boldsymbol{b}) \doteq \frac{1}{2}((\boldsymbol{a} \cdot \nabla)\boldsymbol{b} + (\boldsymbol{b} \cdot \nabla)\boldsymbol{a})$. Note that the perturbation $\epsilon_o P$ modifying $R(i\omega_0)^{-1}$ into Φ at leading order is compensated for at third order. Terms are then collected at each order in $\sqrt{\epsilon_o}$, leading to a cascade of linear problems, detailed hereafter.

At order $\sqrt{\epsilon_o}$, we collect $(\mathrm{i}m\omega_o I - L)\bar{\boldsymbol{u}}_{1,m} = \boldsymbol{0}$ for $m = 0, 2, 3, \ldots$, and $\Phi\bar{\boldsymbol{u}}_{1,1} = \boldsymbol{0}$. Since L is strictly stable, the unforced equation for $m \neq 1$ can only lead to $\bar{\boldsymbol{u}}_{1,m} = \boldsymbol{0}$. Conversely, the kernel of Φ contains the optimal response $\hat{\boldsymbol{u}}_o$, therefore $\bar{\boldsymbol{u}}_{1,1}(T) = A(T)\hat{\boldsymbol{u}}_o$, where $A(T) \in \mathbb{C}$ is a slowly varying scalar amplitude verifying $\partial_t A = 0$. Finally, the general solution at order $\sqrt{\epsilon_o}$ is written

$$
\boldsymbol{u}_1(t, T) = A(T)\hat{\boldsymbol{u}}_o\mathrm{e}^{\mathrm{i}\omega_o t} + \text{c.c.}. \tag{2.9}
$$

At order ϵ_o, we obtain the solution $\boldsymbol{u}_2 = |A|^2\boldsymbol{u}_{2,0} + (A^2\mathrm{e}^{2\mathrm{i}\omega_o t}\hat{\boldsymbol{u}}_{2,2} + \text{c.c.})$, where

$$
\left.\begin{aligned}
-L\boldsymbol{u}_{2,0} &= -2C(\hat{\boldsymbol{u}}_o, \hat{\boldsymbol{u}}_o^*), \\
(2\mathrm{i}\omega_o I - L)\hat{\boldsymbol{u}}_{2,2} &= -C(\hat{\boldsymbol{u}}_o, \hat{\boldsymbol{u}}_o).
\end{aligned}\right\} \tag{2.10}
$$

The homogeneous solution of the system $\Phi\bar{\boldsymbol{u}}_{2,1} = \boldsymbol{0}$ is arbitrarily proportional to $\hat{\boldsymbol{u}}_o$, and written $A_2(T)\hat{\boldsymbol{u}}_o$. It can be ignored ($\bar{\boldsymbol{u}}_{2,1} = \boldsymbol{0}$) without loss of generality. It could also be kept, provided it is included in the definition of the amplitude, which would then become $A + \epsilon_o A_2$.

At order $\sqrt{\epsilon_o}^3$, we assemble two equations yielding the Fourier components of the solution oscillating at ω_o

$$
\Phi\bar{\boldsymbol{u}}_{3,1} = -A|A|^2\left[2C(\hat{\boldsymbol{u}}_o, \boldsymbol{u}_{2,0}) + 2C(\hat{\boldsymbol{u}}_o^*, \hat{\boldsymbol{u}}_{2,2})\right] - \hat{\boldsymbol{u}}_o\frac{\mathrm{d}A}{\mathrm{d}T} - A\hat{\boldsymbol{f}}_o + \phi\hat{\boldsymbol{f}}_h \tag{2.11}
$$

(recalling $P\hat{\boldsymbol{u}}_o = \hat{\boldsymbol{f}}_o$) and at $3\omega_o$, $(3\mathrm{i}\omega_o I - L)\bar{\boldsymbol{u}}_{3,3} = 2A^3 C(\hat{\boldsymbol{u}}_o, \hat{\boldsymbol{u}}_{2,2})$. The operator Φ being singular, the only way for $\bar{\boldsymbol{u}}_{3,1}$ to be non-diverging, and thus for the asymptotic expansion to make sense, is that the right-hand side of (2.11) has a null scalar product with the kernel of $\Phi^\dagger$, i.e. is orthogonal to the adjoint mode $\hat{\boldsymbol{f}}_o$ associated with $\hat{\boldsymbol{u}}_o$. This is known as the

947 A43-8

'Fredholm alternative.' As a result, the amplitude $A(T)$ satisfies

$$\frac{1}{\eta}\frac{\mathrm{d}A}{\mathrm{d}T} = \phi\gamma - A - \frac{\mu + \nu}{\eta}A\,|A|^2\,, \tag{2.12}$$

with the coefficients

$$\left.\begin{array}{cc} \eta = \dfrac{1}{\left\langle \hat{\boldsymbol{f}}_o, \hat{\boldsymbol{u}}_o \right\rangle}, & \gamma = \left\langle \hat{\boldsymbol{f}}_o, \hat{\boldsymbol{f}}_h \right\rangle, \\[2ex] \dfrac{\mu}{\eta} = \left\langle \hat{\boldsymbol{f}}_o, 2C(\hat{\boldsymbol{u}}_o, \boldsymbol{u}_{2,0}) \right\rangle, & \dfrac{\nu}{\eta} = \left\langle \hat{\boldsymbol{f}}_o, 2C(\hat{\boldsymbol{u}}_o^*, \hat{\boldsymbol{u}}_{2,2}) \right\rangle. \end{array}\right\} \tag{2.13}$$

The coefficient γ is the projection of the applied forcing on the optimal forcing. The coefficient μ embeds the interaction between $\hat{\boldsymbol{u}}_o$ and the static perturbation $\boldsymbol{u}_{2,0}$, i.e. it corrects the gain according to the fact that $\hat{\boldsymbol{u}}_o$ extracts energy from the time-averaged mean flow rather than from the original base flow. In contrast, the coefficient ν embeds the interaction between $\hat{\boldsymbol{u}}_o^*$ and the second harmonic $\hat{\boldsymbol{u}}_{2,2}$. We show in Appendix A that, in the regime of small variations around the linear gain, the amplitude equation reduces to the standard sensitivity of the gain (Brandt *et al.* 2011) to a base flow modification induced by $\boldsymbol{u}_{2,0}$, and embeds the effect of the second harmonic $\hat{\boldsymbol{u}}_{2,2}$ as well. Introducing the rescaled quantities $a \doteq \sqrt{\epsilon_o}A$ and $F = \phi\sqrt{\epsilon_o}^3$, such that the weakly nonlinear harmonic gain $G = \|\sqrt{\epsilon_o}\bar{\boldsymbol{u}}_{1,1}\|/\|\phi\sqrt{\epsilon_o}^3\hat{\boldsymbol{f}}_h\|$ is simply $= |a|/F$, (2.12) becomes

$$\frac{1}{\eta\epsilon_o}\frac{\mathrm{d}a}{\mathrm{d}t} = \frac{\gamma F}{\epsilon_o} - a - \frac{\mu + \nu}{\eta\epsilon_o}a\,|a|^2\,. \tag{2.14}$$

The gain associated with the linearised version of (2.14) is $G = |\gamma|/\epsilon_o$, as expected for the linear prediction. We recover $G = 1/\epsilon_o$ when the optimal forcing is applied ($\gamma = 1$). We also note that this expression predicts $G = 0$ when $\gamma = 0$, which merely indicates that the linear response is orthogonal to $\hat{\boldsymbol{u}}_o$, without stating anything on the gains associated with sub-optimal forcings except that they should be at most $O(\epsilon_o^{-1/2})$, assuming a sufficiently large 'spectral' gap in the singular-value decomposition of the resolvent operator. For the rest of the paper, we set $\gamma = 1$. Expressing a in terms of an amplitude $|a| \in \mathbb{R}^+$ and a phase $\rho \in \mathbb{R}$ such that $a(t) = |a(t)|\mathrm{e}^{\mathrm{i}\rho(t)}$, the time-independent equilibrium solutions, or fixed points, of (2.14), $(|a_e|, \rho_e)$, solve

$$\frac{F}{\epsilon_o}\mathrm{e}^{-\mathrm{i}\rho_e} = |a_e| + \frac{\mu + \nu}{\eta\epsilon_o}\,|a_e|^3\,. \tag{2.15}$$

Squaring and adding the real and imaginary parts of (2.15) leads to a third-order polynomial for the equilibrium amplitude of (2.14)

$$DY^3 + 2BY^2 + Y = \left(\frac{F}{\epsilon_o}\right)^2 \quad \text{with} \quad D = \frac{|\mu + \nu|^2}{\epsilon_o^2\,|\eta|^2} > 0 \quad \text{and} \quad B = \mathrm{Re}\left[\frac{\mu + \nu}{\epsilon_o\eta}\right], \tag{2.16}$$

and where $Y = |a_e|^2 > 0$. Let $p(Y) = DY^3 + 2BY^2 + Y$ be the left-hand side of (2.16). We further distinguish two cases: (i) if $B \geq 0$, $p(Y)$ is increasing monotonically with Y and can only cross the constant line $(F/\epsilon_o)^2$ once. We have in addition $p(Y) > Y$, thus the gain smaller than the linear prediction and monotonically decaying while F is increasing. Conversely, if (ii) $B < 0$, we have $p(Y) < Y$ in the interval $0 < Y < -2B/D$, and the

gain should then be greater than the linear one in the corresponding range of forcing $0 < (F/\epsilon_o)^2 < -2B/D$. Furthermore, $p(Y)$ may vary non-monotonically over this interval and cross the constant line $(F/\epsilon_o)^2$ three times (leading to three solutions for Y); namely, $p(Y)$ may be decreasing on a certain interval of Y while dominated by the negative term $\propto Y^2$, bridging two other intervals where $p(Y)$ is increasing due to the respective positive terms $\propto Y$ and $\propto Y^3$. A necessary and sufficient condition for such a case to occur is that the equation $\mathrm{d}P/\mathrm{d}Y = 3DY^2 + 4BY + 1 = 0$ possesses two real and positive solutions. This is guaranteed if and only if the determinant $\Delta \doteq 16B^2 - 12D$ is strictly positive. Finally, for $-2B/D \leq Y$, $p(Y)$ must be monotonically increasing again with $p(Y) \geq Y$, resulting in a gain smaller than the linear one and monotonically decreasing while F is increasing.

The stability of the equilibrium solution(s) $(|a_e|, \rho_e)$ can also be established from the amplitude equation (2.14). If an equilibrium becomes unstable for a given forcing amplitude, we expect the flow response to depart from the associated limit cycle. However, the stability of the equilibria of the amplitude equation does not directly conclude on stability of the limit cycle, for instance, to perturbations in the third dimension, which could be assessed with a Floquet stability analysis or a direct numerical simulation. Equation (2.14) can be expressed as a two-by-two amplitude/phase nonlinear dynamical system

$$\frac{\mathrm{d}\,|a|}{\mathrm{d}t} = F\left[\eta_r \cos(\rho) + \eta_i \sin(\rho)\right] - \eta_r \epsilon_o\,|a| - (\mu_r + \nu_r)\,|a|^3 \tag{2.17}$$

$$|a|\,\frac{\mathrm{d}\rho}{\mathrm{d}t} = F\left[\eta_i \cos(\rho) - \eta_r \sin(\rho)\right] - \eta_i \epsilon_o\,|a| - (\mu_i + \nu_i)\,|a|^3. \tag{2.18}$$

Perturbing this system around the equilibrium solution $(|a_e|, \rho_e) + (|a|'(t), \rho'(t))$ and neglecting nonlinear terms leads to the following equation for the perturbation $d_t(|a|', \rho')^{\mathrm{T}} = J(|a|', \rho')^{\mathrm{T}}$, where J is the Jacobian matrix expressed as

$$J = \begin{bmatrix} -\epsilon_o\eta_r - 3(\mu_r + \nu_r)\,|a_e|^2 & F\left[\eta_i \cos(\rho_e) - \eta_r \sin(\rho_e)\right] \\ -\epsilon_o\eta_i\,|a_e|^{-1} - 3(\mu_i + \nu_i)\,|a_e| & -F\left[\eta_i \sin(\rho_e) + \eta_r \cos(\rho_e)\right]\,|a_e|^{-1} \end{bmatrix}. \tag{2.19}$$

If at least one of the two eigenvalues of J has a positive real part, the associated equilibrium is linearly unstable.

Note that (2.17) and (2.18), for the amplitude and the phase of the oscillating linear response, are similar to those that would be obtained for a classical Duffing–Van der Pol oscillator with appropriate parameters and harmonically forced around its natural frequency. If the latter is set to one, $\eta_r \epsilon_o$ and $\eta_i \epsilon_o$ are respectively proportional to the damping ratio and the detuning parameter. The coefficient $(\mu_i + \nu_i)$ is proportional to the cubic stiffness parameter (Duffing nonlinearity $\propto x^3$), and $(\mu_r + \nu_r)$ to the nonlinear damping parameter (Van der Pol nonlinearity $\propto \dot{x}x^2$).

For the sake of completeness, Appendix C shows how to compute higher-order corrections of (2.14). It is worth mentioning, in particular, that the Fredholm alternative ensures that higher-order solutions oscillating at ω_o are orthogonal to the optimal response $\hat{\boldsymbol{u}}_o$, and that the action of Φ need not be computed explicitly and can be replaced by the action of $(\mathrm{i}\omega_o I - L)$ for all practical purposes.

2.1. *Application case: the flow past a BFS*

Equation (2.14) is the first main result of this study and will be further referred to as the Weakly Nonlinear Non-normal harmonic (WNNh) model. We discuss its performance
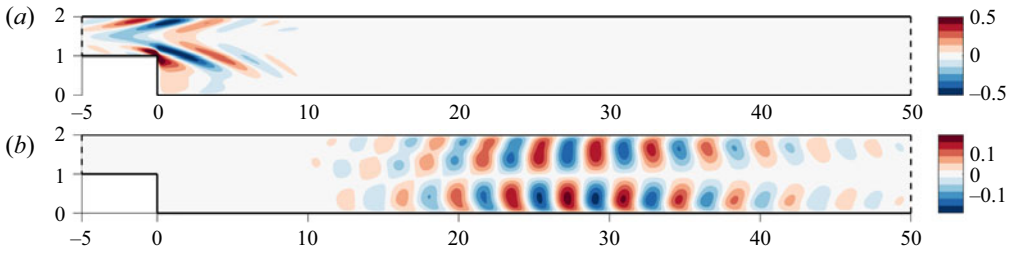
Figure 4. (*a*) Streamwise (*x*) component of the optimal harmonic forcing structure $\mathrm{Re}(\hat{\boldsymbol{f}}_o)$ for the BFS (sketched in figure 2*a*) at $Re = 500$ and at the optimal forcing frequency $\omega_o/(2\pi) = \omega_{o,m}/(2\pi) = 0.075$. (*b*) Streamwise component of the associated response $\mathrm{Re}(\hat{\boldsymbol{u}}_o)$. Both structures are normalised as $\|\hat{\boldsymbol{f}}_o\| = \|\hat{\boldsymbol{u}}_o\| = 1$.

Re	ϵ_0	η	$\mu/(\epsilon_o \eta)$	$\nu/(\epsilon_o \eta)$	B
200	73.9^{-1}	$3.66 - \mathrm{i} \times 0.0163$	$5.13 - \mathrm{i} \times 1.32$	$0.137 + \mathrm{i} \times 1.13$	5.27
500	7456.6^{-1}	$117.1 - \mathrm{i} \times 0.653$	$8.23 - \mathrm{i} \times 2.60$	$0.364 - \mathrm{i} \times 0.396$	8.59
700	148080^{-1}	$1626.7 - \mathrm{i} \times 8.65$	$9.06 - \mathrm{i} \times 4.38$	$-0.729 - \mathrm{i} \times 1.39$	8.33

Table 1. The WNNh coefficients for the BFS flow, when the optimal forcing structure ($\gamma = 1$) is applied at the optimal frequency $\omega_o/(2\pi) = \omega_{o,m}/(2\pi) = 0.075$.

when the stationary flow past a BFS sketched in figure 2 is forced harmonically with the optimal structure $\hat{\boldsymbol{f}}_o$. At $Re = 500$ and the optimal forcing frequency, $\hat{\boldsymbol{f}}_o$ is shown in figure 4(*a*) together with its associated response $\hat{\boldsymbol{u}}_o$ in figure 4(*b*) (see Appendix B for details about the geometry and the numerical method). As shown in Blackburn *et al.* (2008); Boujo & Gallaire (2015), the BFS flow constitutes a striking illustration of streamwise non-normality. As seen in figure 4(*a*), the optimal forcing structure is located upstream and triggers a spatially growing response along the shear layer adjoining the recirculation region, as the result of the convectively unstable nature of the shear layer. We first set the Reynolds number Re between 200 and 700, and the frequency $\omega_o = 2\pi \times 0.075$ close to the most linearly amplified frequency $\omega_{o,m}$, which varies only slightly with Re. The linear gain grows exponentially with Re (Boujo & Gallaire 2015), as seen in table 1. Since η scales like $O(\epsilon_o^{-1/2})$, the term in $\mathrm{d}A/\mathrm{d}T$ in (2.11) is asymptotically consistent only close to equilibrium points where $\mathrm{d}A/\mathrm{d}T = 0$, which is the regime of primary interest in the context of harmonic forcing. In accordance, the temporal derivative $\mathrm{d}A/\mathrm{d}T$ is kept in (2.12) to assess the stability of such equilibria, determined by the analysis of the Jacobian matrix (2.19).

Predictions from the WNNh model are compared with fully nonlinear gains extracted from direct numerical simulations (DNS) in figure 5(*a*). The DNS gains are the ratio between the temporal root-mean-square (r.m.s.) of the kinetic energy of the fluctuations at ω_o (extracted through a Fourier transform) and the r.m.s. of the kinetic energy of the forcing (for instance, the forcing $F\hat{\boldsymbol{f}}_o \mathrm{e}^{\mathrm{i}\omega_o t} + \mathrm{c.c.}$, with $\|\hat{\boldsymbol{f}}_o\| = 1$ corresponding to an effective forcing r.m.s. amplitude of $\sqrt{2}F$). Since the coefficient B defined in (2.16) is strictly positive for all Re, the WNNh model predicts nonlinearities to saturate the energy of the response, and thus the gain to decrease monotonically with the forcing amplitude. This is confirmed by the comparison with DNS, displaying an excellent overall agreement. As shown in the inset (in logarithmic scale), the nonlinear gain transitions
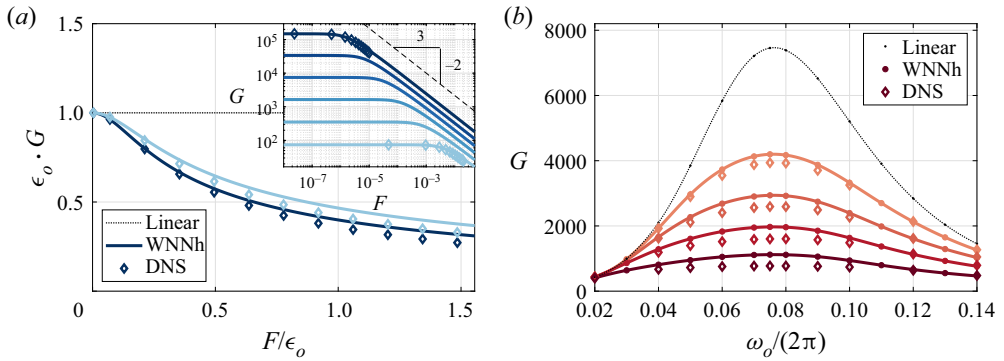
Figure 5. Weakly and fully nonlinear harmonic gain in the BFS flow (sketched in figure 2a). At each frequency and each Reynolds number, the optimal linear forcing structure $\hat{f}_o$ is applied. (a) Fixed frequency $\omega_o/(2\pi) = 0.075$, varying Reynolds number $Re = 200$ and 700 (larger Re darker). Inset: log–log scale, $Re = 200, 300, \ldots, 700$. (b) Fixed Reynolds number $Re = 500$, varying forcing r.m.s. amplitude $F = \sqrt{2}^{-1}[1, 2, 4, 10] \times 10^{-4}$ (larger amplitudes darker).

from a constant value in the linear regime to a $-2/3$ power-law decay when nonlinearities prevail, as predicted from (2.14). This transition is delayed when the Reynolds number (and therefore the linear gain) decreases, and compares well with DNS data. The main plot (in linear scale) confirms the agreement with the DNS, and the improvement over the linear model. Re-scaled WNNh curves appear similar for $Re = 200$ and $Re = 700$, and a slight overestimate is observed as the forcing amplitude approaches ϵ_0. Indeed, $F \sim \epsilon_0$ implies $\phi \sim 1/\sqrt{\epsilon_o}$, which jeopardises the asymptotic hierarchy. Nonetheless, the error remains small for this flow in the considered range of forcing amplitudes. Further physical insight is gained from the WNNh coefficients gathered in table 1. The nonlinear coefficients remain of order one, which confirms the validity of the chosen scalings. The real part of μ being larger than that of ν, the present analysis rationalises *a priori* the predominance of the mean flow distortion over the second harmonic in the saturation mechanism reported *a posteriori* in Mantic-Lugo & Gallaire (2016b).

Next, we select $Re = 500$ and report in figure 5(b) harmonic gains as a function of the frequency, for increasing forcing amplitudes. At each frequency, the corresponding optimal forcing structure $\hat{f}_o$ is applied. The comparison between DNS and WNNh is conclusive over the whole range of frequencies. The saturating character of nonlinearities is well captured. Such a good agreement may appear surprising in the low-frequency regime, for instance at $\omega_o/(2\pi) = 0.04$ where the second harmonics at frequency $2\omega_0$ could, in principle, be amplified approximately four times more than the fundamental. It happens, however, that the associated forcing structure $-C(\hat{u}_o, \hat{u}_o)$ is located much farther downstream than the optimal forcing at $2\omega_o$, with a weak overlap region which results in a poor projection. Therefore, the second-order contribution does not reach amplitudes of concern in this flow, as a consequence of its streamwise non-normality. For $\omega_o/(2\pi) = 0.075$ the fully nonlinear and predicted weakly nonlinear structures are compared in figure 6. The energy centroid of the fully nonlinear response shows a clear migration upstream when increasing the forcing amplitude, as already reported in Mantic-Lugo & Gallaire (2016b). It is associated with a shortening of the mean recirculation bubble under the action of the Reynolds stresses, in turn explaining the reduction of the gain. Although some distortion of the structures due to higher harmonics is observed when increasing the forcing amplitude, the fully nonlinear structure remains dominated by its
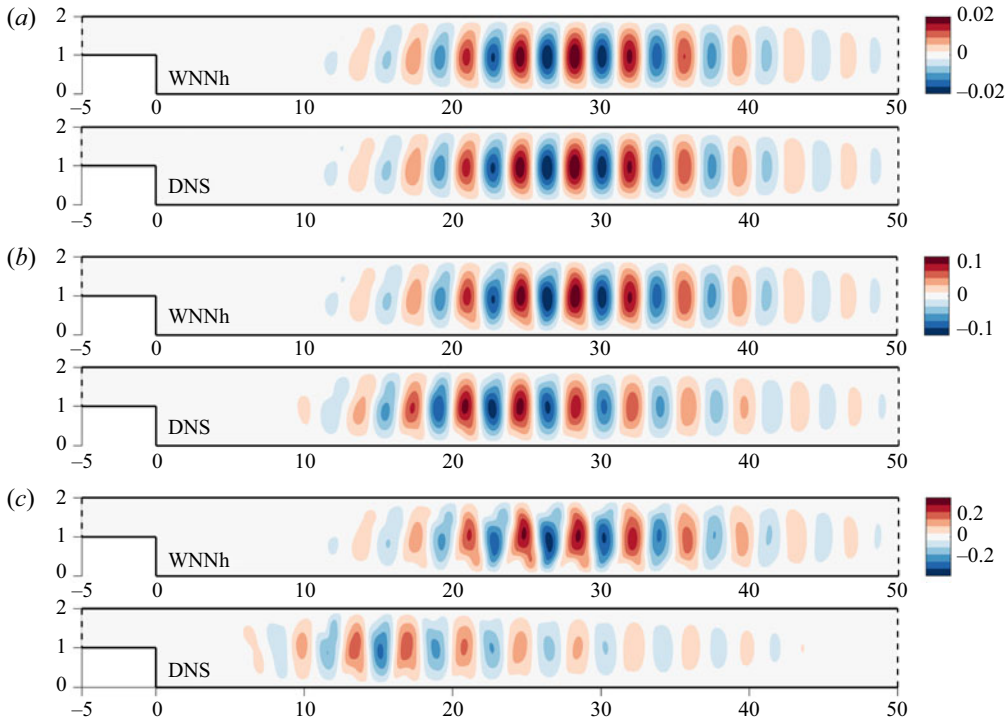
947 A43-12

Figure 6. Snapshots of the weakly (WNNh) and fully (DNS) nonlinear cross-wise (y) component of the velocity perturbation around the mean flow in the BFS flow. The frequency is fixed to $\omega_o/(2\pi) = 0.075$ and the Reynolds number to $Re = 500$. Three increasing forcing amplitudes are considered: (a), (b) and (c) correspond respectively to $F = [10^{-5}, 10^{-4} \text{ and } 10^{-3}]/\sqrt{2}$. The WNNh structures are evaluated as $2\text{Re}(\sqrt{\epsilon_o}A\text{e}^{\text{i}\omega_o t}\hat{\boldsymbol{u}}_o + \epsilon_o A^2 \text{e}^{2\text{i}\omega_o t}\hat{\boldsymbol{u}}_{2,2})$, with A the equilibrium solution of (2.12); the DNS structures are obtained by taking the $n\omega_o$ ($n = 1, 2, 3, \ldots$) Fourier components of a DNS simulation in the stationary regime, then by taking two times the real part of their sum weighted by $\text{e}^{\text{i}n\omega_o t}$. In this manner, the phases can also be compared between WNNh and DNS.

ω_o-component. The weakly nonlinear structure does not capture the upstream migration since it does not include the $O(\epsilon_o^{3/2})$ corrections of the ω_o-component structure; thus, the latter is intrinsically restricted to $\hat{\boldsymbol{u}}_o$. However, the coefficient $\mu + \nu$ is constructed on forcing terms at $O(\epsilon_o^{3/2})$ and indeed embeds the nonlinear interactions responsible for the migration and the saturation, explaining why the predicted level of energy is correct even though the structure is not.

2.2. *Application case: Orr mechanism in the plane Poiseuille flow*

The weakly nonlinear evolution of the harmonic gain is now sought for the plane Poiseuille flow sketched in figure 2, a typical flow with component-wise non-normality (Trefethen *et al.* 1993; Schmid 2007). Periodicity is imposed in the streamwise and spanwise directions with wavenumbers k_x and k_z, respectively. The set of parameters $(Re, k_x, k_z) = (3000, 1.2, 0)$ is selected. According to the classical work of Orszag (1971), the base flow at this Re number is linearly stable since instability first occurs at $Re_{cr} \approx 5772$ and $k_{x,cr} \approx 1.02$. In both the linear and nonlinear computations, the spanwise invariance $k_z = 0$ is systematically maintained. While the base flow $U(y)$ has only one velocity component and depends only on one coordinate, the perturbations are here two-dimensional (i.e.
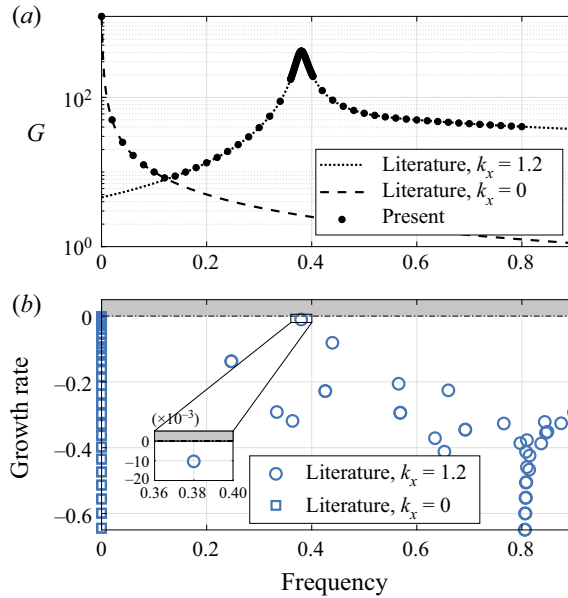
947 A43-13

Figure 7. (*a*) Linear harmonic (optimal) gain as function of the optimisation frequency. Present results are compared with those reproduced from Schmid & Henningson (2001), where perturbations are expressed as Fourier mode of streamwise wavenumber k_x. (*b*) Eigenspectra.

$\boldsymbol{u} = (u_x(x, y), u_y(x, y)))$. The computations are performed in the streamwise-periodic box $(x, y) \in [0, 2\pi/1.2] \times [-1, 1] \equiv \Omega$. All the scalar products are taken upon integration inside this periodic box, in particular for the normalisation $\langle \hat{\boldsymbol{u}}_o, \hat{\boldsymbol{u}}_o \rangle = \langle \hat{\boldsymbol{f}}_o, \hat{\boldsymbol{f}}_o \rangle = 1$, and latter for the evaluation of the weakly nonlinear coefficients.

The linear optimal gain (2.1) is computed in the frequency interval $0 \le \omega_o \le 0.8$ (figure 7*a*), together with the associated optimal forcing and responses structures. Results are validated with the one-dimensional results of Schmid & Henningson (2001) based on a Fourier expansion of wavenumbers $k_x = 1.2$ and $k_x = 0$ in the streamwise direction. Eigenspectra are also reported in figure 7(*b*). The singular value decomposition (SVD) algorithm applied to the periodic box automatically selects the most amplified wavenumber among all spatial harmonics $n1.2$ with $n = 0, 1, 2, \ldots$. Below $\omega_o \approx 0.12$, the harmonic $0 \times 1.2 = 0$ is dominant due to the concentration of weakly damped eigenvalues along the imaginary axis. The gain $G(\omega_o = 0) = 1216$ is equal to the inverse of the smallest damping rate among all these spatially invariant modes. The large value of the gain associated with those modes is understood considering that the small pressure gradient $(2/Re, 0)^{\mathrm{T}} = (2/3000, 0)^{\mathrm{T}}$ is sufficient to induce the Poiseuille base flow (equal to unity in the centreline). Above $\omega_o \approx 0.12$, the fundamental wavenumber $1 \times 1.2 = 1.2$ prevails. The corresponding harmonic gain presents a local and selective maximum for $\omega_o = 0.38$, certainly linked to the presence of the weakly damped eigenvalue $\sigma_1 = -0.0103 + 0.380i$. Nevertheless, $G(\omega_o = 0.38) = 416$ is significantly larger than $1/0.0103 \approx 97$. This is a direct consequence of the non-normality of the plane Poiseuille flow. Unlike the BFS flow, the non-normality at play here is not due to the presence of a convectively unstable region but to the Orr mechanism, suggested for the first time in Orr (1907). Namely, an initial condition or forcing field constituted of spanwise vortices tilted towards the upstream direction (figure 8*a*), tilts downstream under the action of the mean shear (figure 8*b*), which leads to a significant gain in the kinetic energy of
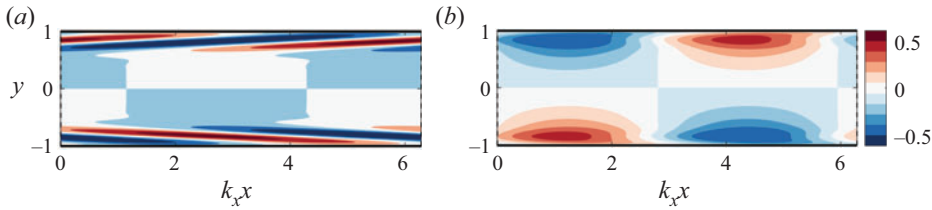
Figure 8. (*a*) Streamwise component of the optimal forcing Re($f_{o,x}$) for the plane Poiseuille flow (sketched in figure 2*b*) for (Re, k_x, k_z) = (3000, 1.2, 0) and $\omega_o = 0.3810$. (*b*) Streamwise component of the response Re($\hat{u}_{o,x}$). Both fields are normalised as $\|\hat{\boldsymbol{f}}_o\| = \|\hat{\boldsymbol{u}}_o\| = 1$. Only one wavelength $0 \leq k_x x \leq 2\pi$ is shown.

ω_o	ϵ_o	η	$\mu/(\epsilon_o\eta)$	$\nu/(\epsilon_o\eta)$	B
0.3810	$(415.6)^{-1}$	$4.06 + \text{i} \times 0.218$	$-177.0 - \text{i} \times 315.6$	$-17.4 - \text{i} \times 197.8\text{i}$	-194.4
0.4025	$(190.4)^{-1}$	$2.78 + \text{i} \times 3.89$	$-160.1 + \text{i} \times 24.3$	$-52.3 - \text{i} \times 10.6$	-212.4

Table 2. The WNNh coefficients for the plane Poiseuille flow at (Re, k_x, k_z) = (3000, 1.2, 0), and when the optimal forcing structure ($\gamma = 1$) is applied.

the perturbation. The coefficient B is shown in figure 9(*a*), and the associated WNNh prolongation of the harmonic gain in figure 9(*b*). The coefficient B is negative in the interval $0.378 \leq \omega_o \leq 0.486$, and B and D are such that three equilibrium amplitudes $|a_e|$ exist for some values of F in the sub-interval $0.389 \leq \omega_o \leq 0.428$. Among them, none or only one is found to be stable. Consequently, as the forcing amplitude is increased, the harmonic gain curve leans toward the higher frequencies in figure 9(*b*); in the meantime, a frequency interval where no stable solution is predicted appears and grows larger.

Note that, in the absence of a stable equilibrium, it is natural to consider completing (2.14) up to $O(\sqrt{\epsilon_o}^5)$. It is shown in Appendix C, however, that such an approach is problematic in the present case, because the non-oscillating forcing terms appearing at $O(\epsilon_o^2)$ excite the largely amplified static modes visible in figure 7 for $\omega_o = 0$. The associated gains being of order $1/\epsilon_o$, the mean flow correction terms at $O(\epsilon_o^2)$ break the asymptotic hierarchy. This problem is not encountered at $O(\epsilon_o)$, because the forcing $-2C(\hat{\boldsymbol{u}}_o, \hat{\boldsymbol{u}}_o^*)$ in (2.10) projects poorly on the optimal one for $\omega_o = 0$, and $\|\boldsymbol{u}_{2,0}\|$ remains of order unity.

For comparison with DNS data, two different forcing frequencies with *a priori* distinct behaviours are selected: $\omega_o = 0.3810$ and $\omega_o = 0.4025$. These two frequencies are highlighted by the vertical dashed grey lines in figure 9. In both cases the coefficient B is negative, and for the case $\omega_o = 0.4025$ three equilibrium solutions exist for some values of F. The linear gains and weakly nonlinear coefficients are reported in table 2.

The corresponding WNNh prolongation of the linear gain as a function of the forcing amplitude is shown in figure 10, together with DNS results. For comparison, the prediction of a 'classical' (modal) amplitude equation constructed around the weakly damped eigenvalue σ_1 and its associated direct and adjoint modes is also added. Its derivation is briefly recalled in Appendix D.

For $\omega_o = 0.3810$ (figure 10*a*), the WNNh gain initially increases with F due to the negativity of B. As visible in table 2, this is mostly due to the contribution of Re$[\mu/(\epsilon_o\eta)]$ which is ten times larger than that of Re$[\nu/(\epsilon_o\eta)]$. Thus, at this frequency, the principal factor for the initial increase of the WNNh gain is the Reynolds stress of the response $a\hat{\boldsymbol{u}}_o$.
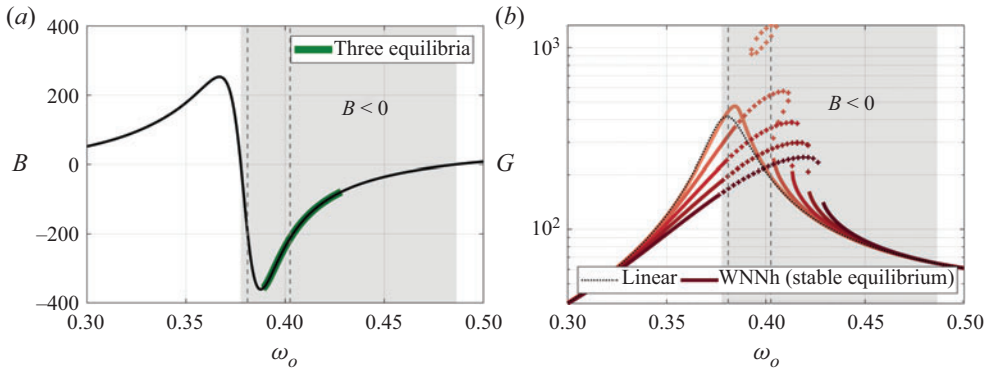
Figure 9. (*a*) Coefficient B defined in (2.16) as a function of the optimisation frequency. The superimposed bold green line indicates that B and D are such that three equilibrium solutions to (2.14) exist. (*b*) Weakly nonlinear harmonic gain predicted by the WNNh model for increasing forcing amplitude F in $[0.55, 1.45, 2.35, 3.25, 4.15] \times 10^{-4}$ (larger F darker). Solid lines denote stable equilibrium solutions of (2.14) whereas bold plus markers (+) denote the unstable ones. The vertical dashed grey lines highlight $\omega_o = 0.3810$ and $\omega_o = 0.4025$, frequencies for which comparison with DNS data is shown in figure 10. The grey zone denotes a negative B.
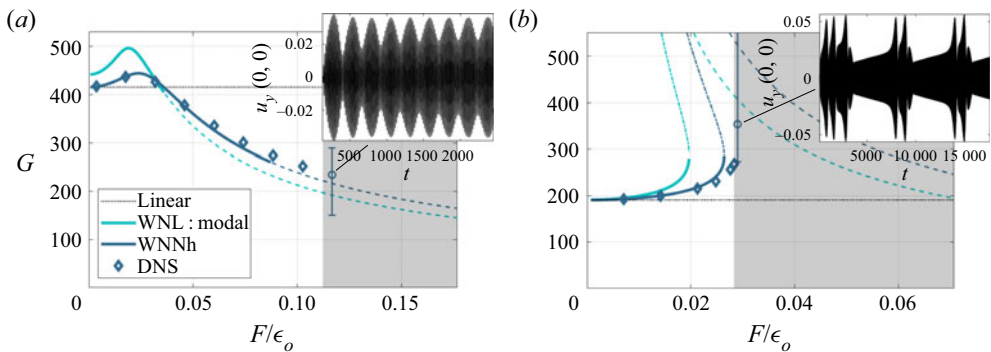

Figure 10. Evolution of the harmonic gain G with respect to F for (*a*) $\omega_o = 0.3810$ and (*b*) $\omega_o = 0.4025$ (frequencies highlighted by vertical dashed grey lines in figure 9). In both, the grey zone indicates that no harmonic gain could be properly defined, as the kinetic energy of the perturbation ceases to converge to a constant value. In particular, the inset shows the monitoring of $u_y(0, 0)$ for the flow represented by the circle (the link is indicated by a thin line).

The latter creates a mean flow that amplifies the linear forcing $\hat{f}_o$ more than the base flow does. This may be interpreted considering the displacement of the eigenvalue σ_1. Let $\hat{q}_1$ (respectively $\hat{a}_1$) denote the eigenmode (respectively adjoint mode) associated with the eigenvalue σ_1. The sensibility of the latter to the base flow deformation δU_b due to the Reynolds stress of $a\hat{u}_o$ is written

$$\delta\sigma_1 = -\frac{\langle \hat{a}_1, C[\hat{q}_1, \delta U_b] \rangle}{\langle \hat{a}_1, \hat{q}_1 \rangle}, \tag{2.20}$$

where $\delta U_b = |a|^2 u_{2,0}$. For $\omega_o = 0.3810$, we obtain $\delta\sigma_1 = |a|^2(1.2 + i \times 3.9)$. Since $\text{Re}[\delta\sigma_1] > 0$, the eigenvalue is moving towards the unstable part of the complex plane under the action of the Reynolds stress. This is in accordance with the fact that the plane Poiseuille flow is subcritical, and may explain the initial increase in the gain with F.

947 A43-16

Meanwhile, $\text{Im}[\delta\sigma_1] > 0$ and σ_1 is shifting toward higher frequencies. Thus ω_o ceases to be the least damped frequency, which could shed light on the fact that increasing F further leads to a monotonic decay in the WNNh gain at ω_o. Because of the flow non-normality, however, this explanation based solely on the location of σ_1 remains qualitative.

The overall agreement with the DNS results is excellent. Nevertheless, the WNNh model slightly underestimates the threshold in F above which a stable equilibrium does not exist anymore. It stands at $F/\epsilon_o = 0.087$ against $F/\epsilon_o = 0.11$ for the DNS. This loss of a proper harmonic response may be symptomatic of the fact that σ_1 eventually crosses the neutral line and becomes unstable. Indeed, for $F/\epsilon_o = 0.11$ (blue circle in the grey zone in figure 10a), the Fourier spectrum of the flow in its stationary regime presents two dominant neighbouring frequencies: the forcing one at $\omega = \omega_o$ and a second 'natural' one at $\omega \approx 0.404$. As these two frequencies are very close, a beating behaviour is visible in the inset of figure 10(a) at a frequency consistent with $\Delta\omega = 0.404 - 0.381 = 0.023$.

The classical modal amplitude equation leads to a prediction that is only qualitative. Even for $F = 0$ the linear harmonic gain $|\langle\hat{\boldsymbol{f}}_o, \hat{\boldsymbol{a}}_1\rangle/(\langle\hat{\boldsymbol{q}}_1, \hat{\boldsymbol{a}}_1\rangle\sigma_{1,r})|$ (see Appendix D for its derivation) is overestimated, as it is deduced from the modal quantities linked to σ_1 only. As mentioned earlier, in non-normal flows a high number of eigenmode is generally necessary to describe its harmonic response, even in the presence of a weakly damped eigenvalue. Thus, relying on a single mode constitutes a poor description of the response to forcing.

We now consider $\omega_o = 0.4025$, and the associated results in figure 10(b). The WNNh model yields multiple equilibrium solutions in the range $0 < F/\epsilon_o < 0.0264$. Only the one represented by a thick continuous line is stable, and corresponds to a monotonic growth of the gain with F. The DNS results validate the existence of this solution. The two other solutions, depicted by the dash-dotted and dashed lines, are unstable in one eigendirection and two eigendirections, respectively. Above $F/\epsilon_o = 0.0264$ the WNNh models predicts the loss of the stable equilibrium solution, which is accurately confirmed by the DNS whose threshold is located around $F/\epsilon_o = 0.0286$. Slightly above, the signal of $u_y(0, 0)$ in the inset suggests again the presence of a 'natural' frequency due to the subcritical destabilisation of σ_1. Indeed, $u_y(0, 0)$ alternates between an algebraic growth typical of a true resonance (both natural and forcing frequencies collapse), and a beating-like behaviour whose period is very long (the natural frequency drifts slightly from the forcing one).

Across this threshold, the evolution of the average kinetic energy of the response appears discontinuous. This loss of a stable equilibrium is to be distinguished with its destabilisation encountered for $\omega = 0.3810$. Overall, the difference of behaviours between figures 10(a) and 10(b) may be explained by the difference of proximity between ω_o and $\text{Im}[\sigma_1]$ of the mean flow. As the forcing is progressively increased above $F/\epsilon_o = 0.0286$, the flow response quickly becomes chaotic, and then turbulent.

It should be mentioned that, in some situations, the amplitude equation (2.14) may be in default. First, as just mentioned, when the optimal linear harmonic gain at frequency $2\omega_o$ is $\sim 1/\sqrt{\epsilon_o}$ or larger and projects well onto the optimal forcing, the asymptotic hierarchy is threatened as $\hat{\boldsymbol{u}}_{2,2}$ may be substantial enough to reach order $\sqrt{\epsilon_o}$ or above. It is thus important to assess that the norm of $\hat{\boldsymbol{u}}_{2,2}$ remains of order one. A second delicate situation arises, for the same reason, when a sub-optimal gain at the frequency ω_o is $\sim 1/\epsilon_o$. In both cases, the model could be extended by including in the kernel of Φ the optimal response at frequency $2\omega_o$, or the sub-optimal response at frequency ω_o, respectively.

Eventually, it should be noted that there are several manners to perturb $R(\text{i}\omega_o)^{-1}$ such as to include $\hat{\boldsymbol{u}}_o$ in the kernel. Among them, the one with the smallest amplitude, i.e. ϵ_o, has been chosen in (2.3). We demonstrate in Appendix E that this is the only choice that leads

947 A43-17

to a consistent amplitude equation. Choosing a higher perturbation amplitude is possible, but implies filling the kernel with another structure than $\hat{\boldsymbol{u}}_o$.

3. Transient growth

Next, we derive an amplitude equation for the weakly nonlinear transient growth in an unforced ($\boldsymbol{f} = \boldsymbol{0}$) system, without restriction on its linear stability.

The solution to the linearised equation (1.2) is $\boldsymbol{u}(t) = \mathrm{e}^{Lt}\boldsymbol{u}(0)$, where e^{Lt} is the operator exponential of Lt. In an unforced context, the propagator e^{Lt} maps an initial structure at time $t = 0$ onto its evolution at $t \geq 0$. The largest linear amplification at $t_o > 0$ (subscript o for 'optimal') is

$$G(t_o) = \max_{\boldsymbol{u}(0)} \frac{\|\boldsymbol{u}(t_o)\|}{\|\boldsymbol{u}(0)\|} = \left\| \mathrm{e}^{Lt_o} \right\| \doteq \frac{1}{\epsilon_o}. \tag{3.1}$$

The singular-value decomposition of the propagator e^{Lt_o} provides the transient gain $G(t_o)$ as the largest singular value of e^{Lt_o}, as well as the left and right singular pair $\boldsymbol{v}_o$ and $\boldsymbol{u}_o$, respectively,

$$\mathrm{e}^{-Lt_o}\boldsymbol{v}_o = \epsilon_o\boldsymbol{u}_o, \quad \left[\left(\mathrm{e}^{Lt_o} \right)^{\dagger} \right]^{-1} \boldsymbol{u}_o = \epsilon_o\boldsymbol{v}_o, \tag{3.2}$$

where $\|\boldsymbol{v}_o\| = \|\boldsymbol{u}_o\| = 1$. The field $\boldsymbol{u}_o$ is the optimal initial structure for the propagation time $t = t_o$, and $\boldsymbol{v}_o$ is its normalised evolution at t_o. The corresponding amplification is $1/\epsilon_o$, as defined in (3.1). Smaller singular values are sub-optimal gains, associated with orthogonal sub-optimal initial conditions. Their orthogonality is ensured by the fact that singular vectors of the operator e^{Lt_o} also are the eigenvectors of the symmetric operator $(\mathrm{e}^{Lt_o})^{\dagger}\mathrm{e}^{Lt_o}$, the singular values of the former being the square root of the eigenvalues of the latter. Of all the t_o, the time leading to the largest optimal gain will be highlighted with the subscript m (for 'maximum') such that $\max_{t_o > 0} G(t_o) = G(t_{o,m})$.

By construction, the linear gain is independent of the amplitude of the initial condition $\boldsymbol{u}(0)$. As this amplitude increases, however, nonlinearities may come into play and the nonlinear gain may depart from the linear gain G. Similar to the previous section on harmonic gain, we propose a method for capturing the effect of weak nonlinearities on the transient gain.

Due to the assumed non-normality of L, the inverse gain is small, $\epsilon_o \ll 1$. While the previous section focused on the inverse resolvent, it is now the inverse propagator e^{-Lt_o} that appears close to singular. The first equality of (3.2) can be rewritten as $(\mathrm{e}^{-Lt_o} - \epsilon_o\boldsymbol{u}_o\langle\boldsymbol{v}_o, *\rangle)\boldsymbol{v}_o = \boldsymbol{0}$, which shows that the operator $(\mathrm{e}^{-Lt_o} - \epsilon_o\boldsymbol{u}_o\langle\boldsymbol{v}_o, *\rangle)$ is singular since $\boldsymbol{v}_o \neq \boldsymbol{0}$ belongs to its kernel. Mirroring our previous reasoning for the WNNh model, we now wish to construct a perturbed inverse propagator whose kernel is the linear trajectory

$$\boldsymbol{l}(t) \doteq \epsilon_o\mathrm{e}^{Lt}\boldsymbol{u}_o, \tag{3.3}$$

seeded by the optimal initial condition $\boldsymbol{u}_o$ and of unit norm in $t = t_o$ since $\boldsymbol{l}(t_o) = \boldsymbol{v}_o$. One conceptual difficulty lies in the fact that the linear response is not a fixed vector field, but a time-dependent trajectory; therefore, the perturbed inverse propagator too should depend on time. We propose to perturb the inverse propagator for all $t \geq 0$ as

$$\Phi(t) = \mathrm{e}^{-Lt} - \epsilon_o P(t), \quad \text{where } P(t) \doteq H(t)\frac{\boldsymbol{u}_o\langle\boldsymbol{l}(t), *\rangle}{\|\boldsymbol{l}(t)\|^2}, \tag{3.4}$$

and where the Heaviside distribution $H(t)$ satisfies $H(0) = 0$ and $H(t > 0) = 1$. As the time $t \to t_o$, the perturbation operator $P \to \boldsymbol{u}_o\langle\boldsymbol{v}_o, *\rangle$ such that $\|P\| \to 1$ and the
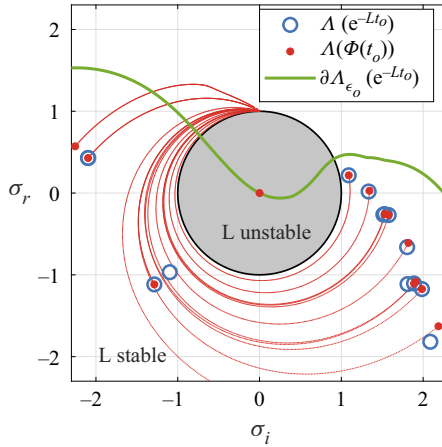
947 A43-18

Figure 11. Restricted spectra (fifteen least stable eigenvalues) of the natural and perturbed inverse propagators of the plane Poiseuille flow (sketched in figure 2b) for $t = t_o = 10$ and $(Re, k_x, k_z) = (3000, 0.5, 2)$ (purely one-dimensional computations using the code of Schmid & Henningson (2001) based on a Fourier expansion of wavenumbers k_x and k_z in x and z, respectively). Blue circles: eigenvalues of e^{-Lt_o}. Red dots: eigenvalues of $\Phi(t_o)$. By construction, one eigenvalue of $\Phi(t)$ lies at the origin. Thin red lines: full locus of the eigenvalues of $\Phi(t)$ for $t \le t_o$. Green line: ϵ_o-pseudospectrum of e^{-Lt_o}, such that $\|(e^{-Lt_o} - zI)^{-1}\| = 1/\epsilon_o$.

expansion (3.4) is certainly justified. The non-trivial kernel of $\Phi(t)$ is $l(t)$ for all $t > 0$; the kernel reduces to $\mathbf{0}$ at $t = 0$ since $\Phi(0) = I$. We show in addition that, for $t > 0$, the non-trivial kernel of the adjoint operator $\Phi(t)^\dagger$ is

$$b(t) \doteq \left(e^{Lt}\right)^\dagger l(t). \tag{3.5}$$

Indeed, using that $P^\dagger = l(t)\langle u_o, * \rangle / \langle l(t), l(t) \rangle$ for $t > 0$, we have

$$\Phi(t)^\dagger b(t) = \left(e^{-Lt}\right)^\dagger b(t) - \epsilon_o l(t) \frac{\langle u_o, b(t) \rangle}{\langle l(t), l(t) \rangle}$$

$$= \left(e^{-Lt}\right)^\dagger b(t) - \epsilon_o l(t) \frac{\langle e^{Lt} u_o, l(t) \rangle}{\langle l(t), l(t) \rangle}$$

$$= \left(e^{-Lt}\right)^\dagger b(t) - l(t)$$

$$= \left[\left(e^{Lt}\right)^\dagger\right]^{-1} b(t) - l(t)$$

$$= \mathbf{0}. \tag{3.6}$$

As an illustration of the singularisation of e^{-Lt_o}, parts of the spectra of e^{-Lt_o} and $\Phi(t_o)$ are shown in figure 11 for the plane Poiseuille flow sketched in figure 2. The red dot at the origin is the null singular eigenvalue of $\Phi(t_o)$ associated with $l(t_o)$. Since $\|P(t_o)\| = 1$, this singular eigenvalue lies on the ϵ_o-pseudospectrum of e^{-Lt_o}, meaning that a perturbation of amplitude ϵ_o is sufficient to make the inverse propagator singular.

Recalling that L is assumed strongly non-normal, we choose $\epsilon_o \ll 1$ as expansion parameter, introduce the slow time scale $T = \epsilon_o t$ and propose the multiple-scale expansion

$$U(t, T) = U_e + \epsilon_o u_1(t, T) + \epsilon_o^2 u_2(t, T) + O(\epsilon_o^3). \tag{3.7}$$

947 A43-19

The square root scaling of the previous section is not made here, as resonance at second order cannot be excluded *a priori*. The flow is initialised with $U(0) = \alpha \epsilon_o^2 u_o$, where $\alpha = O(1)$ is a prefactor. After injecting this expansion in the unforced Navier–Stokes equations, we obtain

$$\epsilon_o(\partial_t - L)u_1 + \epsilon_o^2[(\partial_t - L)u_2 + C(u_1, u_1) + \partial_T u_1] + O(\epsilon_o^3) = 0, \qquad (3.8)$$

subject to $u_2(0) = \alpha u_o$, and $u_i(0) = 0$ for $i \neq 2$. In its primary quality of inverse propagator, the following property holds for e^{-Lt}: $\partial_t(e^{-Lt}) = -e^{-Lt}L$, where the commutation of e^{-Lt} and L has not been used. Thanks to this relation, we write $(\partial_t - L)u_i = e^{Lt}\partial_t(e^{-Lt}u_i)$. As a result, L disappears from the asymptotic expansion but e^{-Lt} appears. The latter is perturbed according to (3.4), leading to $e^{Lt}\partial_t(e^{-Lt}u_i) = e^{Lt}\partial_t(\Phi(t)u_i) + \epsilon_o e^{Lt}\partial_t(P(t)u_i)$ for $i = 1, 2, \ldots$. The asymptotic expansion (3.8) becomes

$$\epsilon_o e^{Lt}\partial_t(\Phi u_1) + \epsilon_o^2\left[e^{Lt}\partial_t(\Phi u_2) + C(u_1, u_1) + \partial_T u_1 + e^{Lt}\partial_t(P(t)u_1)\right] + O(\epsilon_o^3) = 0. \qquad (3.9)$$

Note that the transformation performed from (3.8) to (3.9) is not restricted to time-independent base flows, as the property $\partial_t(\Psi(t)^{-1}) = -\Psi(t)^{-1}L(t)$ holds for a time-varying operator $L(t)$ and the associated propagator $\Psi(t)$. This can be shown easily by taking the time derivative of $\Psi(t)^{-1}u(t) = u(0)$. Terms of (3.9) are then collected at each order in ϵ_o, leading to a succession of linear problems, detailed hereafter.

At order ϵ_o, we collect $\partial_t(\Phi u_1) = 0$, subject to $u_1(0) = 0$. We obtain $\Phi u_1 = \Phi(0)u_1(0) = 0$, therefore $u_1(t, T)$ is proportional to the kernel of $\Phi(t)$ for all $t \geq 0$. We choose the non-trivial solution

$$u_1(t, T) = A(T)H(t)l(t), \qquad (3.10)$$

where the initial condition $u_1(0) = 0$ is enforced by $H(t)$, while the slowly varying scalar amplitude $A(T)$ is continuous in T and modulates the linear trajectory. This choice is motivated by the observation that, since A must be constant in time in the linear regime, we expect it to be weakly time dependent in the weakly nonlinear regime. We stress that $A(T)$ does not depend explicitly on t, such that $\partial_t A = 0$. Note that the choice $u_1(t) = A(t)H(t)l(t)$ would also have been possible, and the assumption of the amplitude depending on a slow time scale is made solely to simplify the ensuing calculations.

At order ϵ_o^2, we collect

$$\partial_t(\Phi u_2) + A^2 H e^{-Lt}C(l, l) + H\frac{dA}{dT}e^{-Lt}l + A d_t(HPl) = 0, \qquad (3.11)$$

subject to $u_2(0) = \alpha u_o$. We used the property $H(t)^2 = H(t)$, which will henceforth be understood. The particular solution of (3.11) yields

$$u_2(t, T) = u_2^{(a)}(t) + A(T)^2 u_2^{(b)}(t) + \frac{dA(T)}{dT}u_2^{(c)}(t) + A(T)u_2^{(d)}(t), \qquad (3.12)$$

where

$$\left.\begin{array}{ll} d_t\left(\Phi u_2^{(a)}\right) = 0, & d_t\left(\Phi u_2^{(b)}\right) = -H e^{-Lt}C(l, l), \\[2mm] d_t\left(\Phi u_2^{(c)}\right) = -H e^{-Lt}l, & \text{and} \quad d_t\left(\Phi u_2^{(d)}\right) = -d_t(HPl), \end{array}\right\} \qquad (3.13)$$

subject to the initial conditions $u_2^{(a)}(0) = \alpha u_o$ and $u_2^{(b)}(0) = u_2^{(c)}(0) = u_2^{(d)}(0) = 0$. Time integration can now be performed without ambiguity as all the partial derivatives $(\partial_t \cdots)$

947 A43-20

have been replaced by total derivatives $(d_t \ldots)$. After time integration between $t = 0$ and $t > 0$, we obtain a series of problems for $\boldsymbol{u}_2^{(a)}$, $\boldsymbol{u}_2^{(b)}$, $\boldsymbol{u}_2^{(c)}$ and $\boldsymbol{u}_2^{(d)}$

$$\Phi(t)\boldsymbol{u}_2^{(a)}(t) = \Phi(0)\boldsymbol{u}_2^{(a)}(0) = \alpha\boldsymbol{u}_o, \tag{3.14}$$

since $\Phi(0) = I$;

$$\Phi(t)\boldsymbol{u}_2^{(b)}(t) = -\int_0^t H(s)\mathrm{e}^{-Ls}C[\boldsymbol{l}(s), \boldsymbol{l}(s)]\,\mathrm{d}s = \mathrm{e}^{-Lt}\tilde{\boldsymbol{u}}_2(t), \tag{3.15}$$

where

$$\frac{\mathrm{d}\tilde{\boldsymbol{u}}_2}{\mathrm{d}t} = L\tilde{\boldsymbol{u}}_2 - C(\boldsymbol{l}, \boldsymbol{l}), \quad \tilde{\boldsymbol{u}}_2(0) = \boldsymbol{0}, \tag{3.16}$$

and where we have used that the general solution of $d_t\boldsymbol{x} = L\boldsymbol{x} + \boldsymbol{F}$ is $\boldsymbol{x}(t) = \mathrm{e}^{Lt}[\boldsymbol{x}(0) + \int_0^t \mathrm{e}^{-Ls}\boldsymbol{F}(s)\mathrm{d}s]$;

$$\Phi(t)\boldsymbol{u}_2^{(c)}(t) = -\int_0^t H(s)\mathrm{e}^{-Ls}\boldsymbol{l}(s)\,\mathrm{d}s$$

$$= -\int_0^t H(s)\epsilon_o\boldsymbol{u}_o\,\mathrm{d}s = -\epsilon_o\boldsymbol{u}_o t, \tag{3.17}$$

since $\mathrm{e}^{-Lt}\boldsymbol{l}(t) = \epsilon_o\boldsymbol{u}_o$ holds by construction; and

$$\Phi(t)\boldsymbol{u}_2^{(d)}(t) = -[H(t)P(t)\boldsymbol{l}(t) - H(0)P(0)\boldsymbol{l}(0)] = -\boldsymbol{u}_o, \tag{3.18}$$

since, by construction, $H(t)P(t)\boldsymbol{l}(t) = H(t)\boldsymbol{u}_o$. Note that the presence of the Heaviside distribution inside the integral is unimportant. Eventually,

$$\Phi\boldsymbol{u}_2 = \alpha\boldsymbol{u}_o + A^2\mathrm{e}^{-Lt}\tilde{\boldsymbol{u}}_2 - \epsilon_o t\frac{\mathrm{d}A}{\mathrm{d}T}\boldsymbol{u}_o - A\boldsymbol{u}_o, \quad t > 0. \tag{3.19}$$

Invoking again the Fredholm alternative, (3.19) admits a non-diverging particular solution if and only if its right-hand side is orthogonal to $\boldsymbol{b}(t)$ for all $t > 0$. This leads to

$$\langle\boldsymbol{u}_o, \boldsymbol{b}(t)\rangle\,(\alpha - A) + A^2\left\langle\mathrm{e}^{-Lt}\tilde{\boldsymbol{u}}_2(t), \boldsymbol{b}(t)\right\rangle - \epsilon_o t\frac{\mathrm{d}A}{\mathrm{d}T}\,\langle\boldsymbol{u}_o, \boldsymbol{b}(t)\rangle = 0, \quad t > 0. \tag{3.20}$$

Dividing (3.20) by $\langle\boldsymbol{u}_o, \boldsymbol{b}(t)\rangle$ leads to

$$(\alpha - A) + \epsilon_o A^2\mu_2(t) - \epsilon_o t\frac{\mathrm{d}A}{\mathrm{d}T} = 0, \quad t > 0, \tag{3.21}$$

where

$$\mu_2(t) = \epsilon_o^{-1}\frac{\left\langle\mathrm{e}^{-Lt}\tilde{\boldsymbol{u}}_2(t), \boldsymbol{b}(t)\right\rangle}{\langle\boldsymbol{u}_o, \boldsymbol{b}(t)\rangle} = \frac{\langle\tilde{\boldsymbol{u}}_2(t), \boldsymbol{l}(t)\rangle}{\langle\boldsymbol{l}(t), \boldsymbol{l}(t)\rangle}. \tag{3.22}$$

Equation (3.21) is re-expressed as $E(t, T) = 0$ for $t > 0$, where $E(t, T) = (\alpha - A) + \epsilon_o A^2\mu_2(t) - \epsilon_o t\mathrm{d}_T A$. Since $\int_{t\to 0}^t \partial_s E(s, T)\,\mathrm{d}s = E(t, T) - E(t \to 0, T)$, solving $E(t, T) = 0$ is equivalent to solving $\partial_t E(t, T) = 0$ for $t > 0$ subject to $E(t \to 0, T) = 0$. Thereby, the partial derivative of (3.21) with respect to the short time scale t is taken, leading to

$$\epsilon_o A^2\frac{\mathrm{d}\mu_2(t)}{\mathrm{d}t} - \epsilon_o\frac{\mathrm{d}A}{\mathrm{d}T} = 0, \quad 0 < t, \tag{3.23}$$

where we have used that $\partial_t A = 0$ by construction since $A = A(T)$ does not explicitly depend on t. Furthermore, the relation (3.23) is subject to $E(t \to 0, T) = \lim_{t \to 0}(\alpha -$

$A) = 0$ where we have used that $\tilde{u}_2(t \to 0) = \tilde{u}_2(0) = 0$. To be meaningful, (3.23) and its initial condition must be re-written solely in terms of t, which is done by evaluating T along $T = \epsilon_o t$. The total derivative of A, denoted $d_t A$, is now needed, as it takes into account the implicit dependence of A on t. By definition, $d_t A = \partial_t A + \epsilon_o \partial_T A = \epsilon_o d_T A$, such that the final amplitude equation reads

$$\frac{dA}{dt} = \epsilon_o A^2 \frac{d\mu_2(t)}{dt}, \quad \text{with } A(0) = \alpha, \tag{3.24}$$

as $\lim_{t \to 0}(\alpha - A(\epsilon_o t)) = 0$ implies $A(t \to 0) = \alpha$, and the amplitude A is extended by continuity in $t = 0$ so as to eventually impose $A(0) = \alpha$. Note that the evaluation in $T = \epsilon_o t$ and the passage to the total derivative would lead to indeterminacy in its solution if performed directly in (3.21), since that equation is not subject to any initial condition. Indeed, at linear level for instance, it would yield $d_t A = (\alpha - A)/t$, which admits the family of solutions $A(t) = \alpha + Ct$, with C an undetermined constant.

We stress that the inverse propagator is not needed to solve the amplitude equation (3.24). Just like the original problem considered in this section, (3.24) is unforced and has a non-zero initial condition. In the linear regime, $A = \alpha$ for all times, and the linear gain is $\|\epsilon_o \alpha l(t)\|/\|\alpha \epsilon_o^2\| = \|l(t)\|/\epsilon_o$. At $t = t_o$, in particular, we recover that it is equal to $1/\epsilon_o$ since $\|l(t_o)\| = \|v_o\| = 1$.

In the following, we call equation (3.24) the Weakly Nonlinear Non-normal transient (WNNt) model. It can be corrected with higher-order terms, which requires solving the linear singular system (3.19), as detailed in Appendix F. We show in particular that singular higher-order solutions are orthogonal to the first-order solution $l(t)$, and that the action of Φ need not be computed explicitly but can in practice be replaced by the action of e^{-Lt}.

3.1. *Application case: the flow past a BFS*

The WNNt model is applied to the BFS flow for $Re = 500$ and $t_o = t_{o,m} = 58$. See Appendix B for details about the numerical method. For these parameters, the linear optimal structures (figure 12) and gain are validated with the results presented in Blackburn *et al.* (2008). The quadratic term in (3.24), although asymptotically correct, happens to be insufficient to capture the nonlinear saturation of the transient gain for this particular flow, in particular because of the weak value of the coefficient $\mu_2(t)$. Indeed, $l(t_o) = v_o$ appears to be dominated by a specific spatial wavenumber (see figure 12b), thus the field $\tilde{u}_2$, being generated by the nonlinear interaction of $l(t)$ with itself, is dominated by spatial harmonics and its projection on $l(t)$ is close to zero. For this flow the WNNt model therefore needs to be extended to order ϵ_o^3 (see Appendix F), yielding

$$\frac{dA}{dt} = \epsilon_o A^2 \frac{d\mu_2}{dt} + \epsilon_o^2 A^3 \frac{d\mu_3}{dt}, \quad A(0) = \alpha, \tag{3.25}$$

where

$$\mu_3(t) \doteq \frac{\langle \tilde{u}_3(t), l(t) \rangle}{\langle l(t), l(t) \rangle}, \tag{3.26}$$

and

$$\frac{d\tilde{u}_3}{dt} = L\tilde{u}_3 - 2\left[C(l, \tilde{u}_2) - \mu_2 C(l, l) + \dot{\mu}_2(\tilde{u}_2 - \mu_2 l)\right], \quad \tilde{u}_3(0) = \mathbf{0}. \tag{3.27}$$

Equation (3.25) is similar to (3.24), although corrected by a cubic term. We formulate the amplitude equation (3.25) in terms of the rescaled quantities $a = \epsilon_o A$ and the amplitude
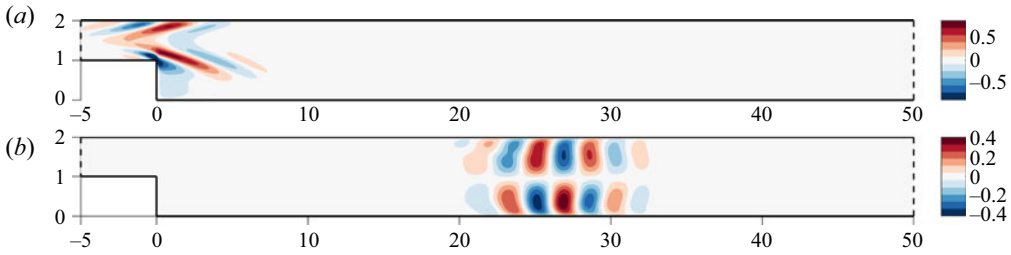
947 A43-22

Figure 12. (*a*) Streamwise (*x*) component of the optimal initial condition $\boldsymbol{u}_o$ for the BFS (sketched in figure 2*a*) at $Re = 500$ and at $t_o = t_{o,m} = 58$. (*b*) Streamwise component of the evolution $\boldsymbol{v}_o$ at $t = t_o$. Both structures are normalised as $\|\boldsymbol{u}_o\| = \|\boldsymbol{v}_o\| = 1$.

of the initial condition $U_0 = \|\boldsymbol{U}(0)\| = \alpha \epsilon_o^2$

$$\frac{\mathrm{d}a}{\mathrm{d}t} = a^2 \frac{\mathrm{d}\mu_2}{\mathrm{d}t} + a^3 \frac{\mathrm{d}\mu_3}{\mathrm{d}t}, \quad a(0) = \frac{U_0}{\epsilon_o}. \tag{3.28}$$

In this manner, the weakly nonlinear transient gain becomes $G(t_o) = a(t_o)/U_0$. Note that in (3.28) the amplitude $a(t)$ does not depend on U_0 nor on ϵ_o independently, but on their ratio U_0/ϵ_o. Thus, as expected, increasingly nonlinear regimes are found when the amplitude of the initial condition increases with respect to the linear gain.

Predictions from (3.28) are shown in figure 13 together with the linear and fully nonlinear DNS gain evaluated as $G_{tot}(t) = \|\boldsymbol{U}(t) - \boldsymbol{U}_e\|/U_0$. In figure 13(*a*), the WNNt model extended to $O(\epsilon_o^3)$ appears to capture the weakly evolution of the transient gain with satisfactory precision. When the amplitude of the initial condition is too large, the higher-order fields $\tilde{\boldsymbol{u}}_2$, $\tilde{\boldsymbol{u}}_3$, ... are expected to have a significant amplitude, and thus the WNNt prediction deteriorates since it is based on an asymptotic hierarchy. In figure 13(*b*), the gain history of $G_{tot}(t)$ for all times $0 \le t \le t_o$ is successfully compared with $a(t)\|\boldsymbol{l}(t)\|/U_0$. The coefficient $\mu_3(t)$ is much larger than $\mu_2(t)$ (inset), and is largely dominated by the part of $\tilde{\boldsymbol{u}}_3$ generated by the forcing term $C(\boldsymbol{l}, \tilde{\boldsymbol{u}}_2)$. Since $\mu_3(t)$ is monotonically decreasing toward $\mu_3(t_o) = -7.77$, larger times are subject to a stronger saturation. This leads to a decrease of the time for which the specific initial condition $\boldsymbol{u}_o$ leads to a maximum transient gain, consistently with the DNS results.

3.2. *Application case: lift-up in the plane Poiseuille flow*

The WNNt is now applied to the plane Poiseuille flow. The set of parameters $(Re, k_x, k_z, t_o) = (3000, 0, 2, t_{o,m} = 230)$ is selected. In both the linear and nonlinear computations, the wavenumber $k_x = 0$ is maintained such that the fields are constant in *x*, and only the dependence in *y* and *z* is computed. Contrarily to the application case § 2.2, perturbations can now be fully three-dimensional (i.e. $\boldsymbol{u} = (u_x(y,z), u_y(y,z), u_z(y,z))$). The computations are performed in the spanwise-periodic box $(y, z) \in [-1, 1] \times [-\pi/2, \pi/2] \equiv \Omega$. All the scalar products are taken upon integration inside this periodic box, in particular for the normalisation $\langle \boldsymbol{u}_o, \boldsymbol{u}_o \rangle = \langle \boldsymbol{v}_o, \boldsymbol{v}_o \rangle = 1$, and for the evaluation of the weakly nonlinear coefficients. The linear optimal gain is validated with the result of Schmid & Henningson (2001); the associated optimal initial condition and its evolution at $t = t_o$ are shown in figures 14(*a*) and 14(*b*), respectively. The optimal initial condition consists of vortices aligned in the streamwise direction; as these streamwise vortices are superimposed on the parabolic base flow, they bring low-velocity fluid from the wall towards the channel centre and high-velocity fluid from the centre of the channel towards
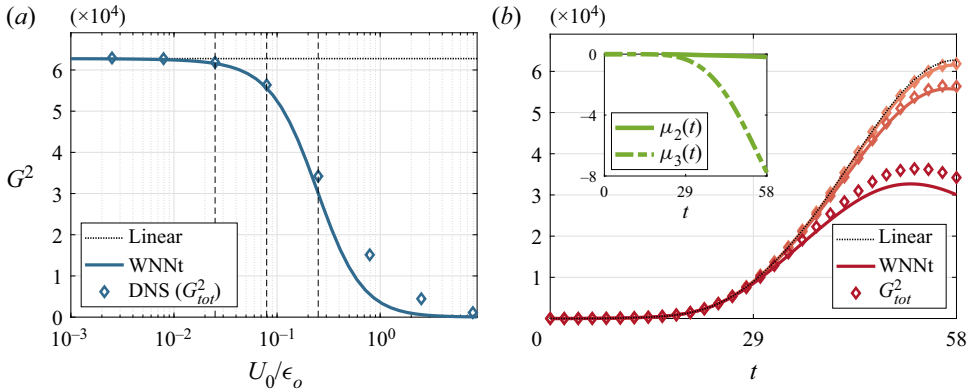
Figure 13. Transient gain in the flow past a BFS (sketched in figure 2a) for $Re = 500$. (a) Gain squared $G(t_o)^2$ for $t_o = t_{o,m} = 58$ as a function of the amplitude of the initial condition. (b) History of the gain squared for $0 \leq t \leq t_{o,m}$ and for three amplitudes of initial condition, $U_0/\epsilon_o = [0.025, 0.08, 0.25]$ (vertical dashed lines in (a)); larger amplitudes darker. Inset: weakly nonlinear coefficients $\mu_2(t)$ (continuous line) and $\mu_3(t)$ (dashed-dotted line) as a function of time.

the walls, thus generating alternated streamwise streaks. Due to the spanwise periodicity of the optimal initial condition $\boldsymbol{u}_o$, all the solutions at even orders ϵ_o^{2n} ($n = 1, 2, 3, \ldots$) only yield even spatial harmonics in k_z and are orthogonal to $\boldsymbol{l}(t)$, such that the coefficient $\mu_2(t)$ defined in (3.22) is null at all times. Therefore, (3.28) reduces to

$$\frac{\mathrm{d}a}{\mathrm{d}t} = a^3 \frac{\mathrm{d}\mu_3}{\mathrm{d}t}, \quad a(0) = \frac{U_0}{\epsilon_o}, \tag{3.29}$$

and $\tilde{\boldsymbol{u}}_3$ solves the simplified equation

$$\frac{\mathrm{d}\tilde{\boldsymbol{u}}_3}{\mathrm{d}t} = L\tilde{\boldsymbol{u}}_3 - 2C(\tilde{\boldsymbol{u}}_2, \boldsymbol{l}), \quad \tilde{\boldsymbol{u}}_3(0) = \boldsymbol{0}. \tag{3.30}$$

The analytical solution of (3.29) is written

$$a(t) = \frac{U_0}{\epsilon_o} \left[1 - \left(\frac{U_0}{\epsilon_o} \right)^2 2\mu_3(t) \right]^{-1/2}. \tag{3.31}$$

We show in Appendix G that, at first order in the gain variation, (3.31) reduces to the sensitivity of the transient gain to the base flow modification $(U_0/\epsilon_o)^2 \tilde{\boldsymbol{u}}_2(t)$.

Predictions from (3.31) are shown in figure 15 together with the linear and fully nonlinear DNS gains. These DNS gains are evaluated in two ways: using either the total perturbation around the base flow, for G_{tot} (already defined), or using only the part of the perturbation fluctuating at k_z along z, for G_{k_z} (in the same manner that we considered only the component oscillating at ω_o in the computation of the gain in the harmonic forcing part). Indeed, $a(t)$ multiplies the linear trajectory field $\boldsymbol{l}(t)$ that is purely fluctuating at k_z along z. The WNNt model predicts G_{k_z} accurately in the weakly nonlinear regime for $t = t_{o,m}$, which supports our approach (figure 15a). In the strongly nonlinear regime, beyond $U_0/\epsilon_o \approx 0.4$, the model overestimates G_{k_z}. This can be interpreted by noting that G_{tot} is twice as large as G_{k_z}, i.e. more energy is contained in the higher-order terms generated by the linear response than in the linear response itself. Therefore, this is not the amplitude equation (3.31) that breaks down, but the very idea of an asymptotic expansion. Whether
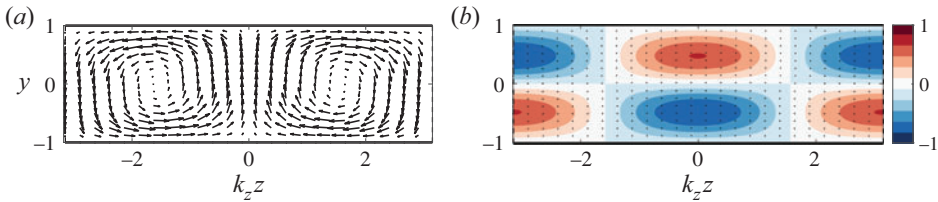
947 A43-24

Figure 14. (*a*) Optimal initial condition $\boldsymbol{u}_o$ for the plane Poiseuille flow (sketched in figure 2*b*) for $(Re, k_x, k_z) = (3000, 0, 2)$ and $t_o = t_{o,m} = 230$. Arrows: cross-sectional velocity field $(u_{o,z}, u_{o,y})$. Contours: streamwise component $u_{o,x}$. (*b*) Evolution $\boldsymbol{v}_o$ at $t = t_o$. Both fields are normalised as $\|\boldsymbol{u}_o\| = \|\boldsymbol{v}_o\| = 1$. Initial vortices have a null streamwise component $u_{o,x}$, and streaks at $t = t_o$ have negligible cross-sectional components $(v_{o,z}, v_{o,y})$. Only one wavelength $-\pi \le k_z z \le \pi$ is shown.
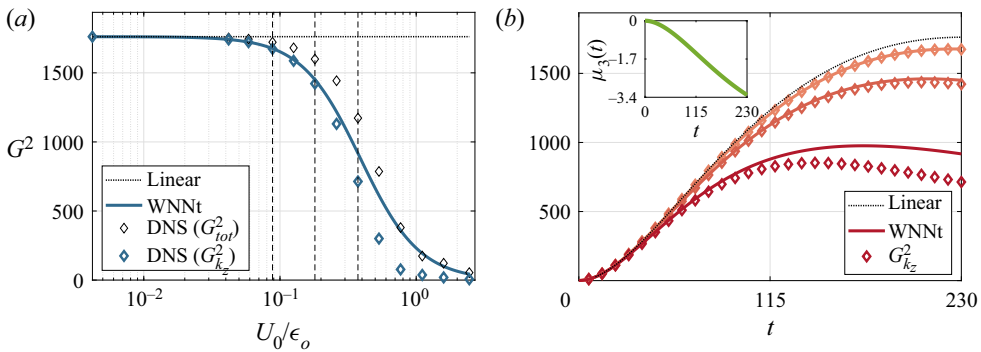

Figure 15. Transient gain in the plane Poiseuille flow (sketched in figure 2*b*) for $(Re, k_x, k_z) = (3000, 0, 2)$. (*a*) Gain squared $G(t_o)^2$ for $t_o = t_{o,m} = 230$ as a function of the amplitude of the initial condition. Streamwise invariance $k_x = 0$ is enforced in the DNS as well. (*b*) History of the gain squared for $0 \le t \le t_{o,m}$ and for three amplitudes of initial condition, $U_0/\epsilon_o = [0.088, 0.18, 0.37]$ (vertical dashed lines in (*a*)); larger amplitudes darker. Inset: weakly nonlinear coefficient $\mu_3(t)$ as a function of time.

higher-order terms remain smaller than the fundamental is certainly flow dependent, and the WNNt model is expected to be even more accurate when this is the case, as shown in § 3.1 for the flow past a BFS, which generated rather weak higher-order fields.

Figure 15(*b*) compares for $t \le t_o$ the history of the approximated gain $a(t)\|\boldsymbol{l}(t)\|/U_0$ with that of the DNS gain G_{k_z}, and shows a convincing overall agreement. The coefficient $\mu_3(t)$ is negative and decays monotonically with time until $\mu_3(t_o) = -3.30$ (inset), enhancing the saturation. This results in a reduction of the approximated optimal time with the amplitude of the initial condition, as also observed in the DNS.

The impact of the optimisation time t_o (and therefore the one of ϵ_o) on the WNNt predictions is studied in figure 16. The weakly nonlinear evolution of the gain envelope for an increasing amplitude of the initial condition is reported together with DNS data. For each optimisation time, the (linear) corresponding optimal initial condition is applied. The agreement between WNNt and DNS is satisfactory over the whole range of optimisation times t_o, particularly those associated with lower linear gain as they require higher U_0 to reach a fully nonlinear regime; on the contrary, optimisation times for which the linear gains are large are subject to a more pronounced degradation of the predictions in the considered range of U_0. However, the decrease of both the maximum gain and the time for which it is reached is well captured by the WNNt model.
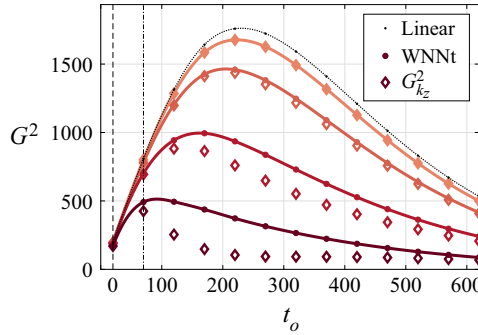
Figure 16. Gain envelope in the plane Poiseuille flow for $Re = 3000$ and $k_x = 0$ (maintained in the DNS as well); the numerical box has a length of π and periodic boundary conditions in the spanwise (z) direction, so the optimisation algorithm automatically select the most amplified wavenumber among all harmonics $k_z = 2n$ with $n = 1, 2, \ldots$. Optimisation times are $t_o = 20, 70, 120, \ldots, 620$: the times $t_o = 20$ (horizontal dashed line), $t_o = 70$ (horizontal dashed-dotted line) and $t_o \geq 120$ correspond respectively to $k_z = 6$, $k_z = 4$ and $k_z = 2$. Four amplitudes of initial condition, $U_0/\epsilon_{o,m} = [0.088, 0.18, 0.37, 0.77]$ are selected, the larger amplitudes are darker.

4. Conclusions

In summary, we have derived two amplitude equations for non-normal systems, describing the asymptotic response to harmonic forcing and the transient response to initial condition. In both cases, the presence of a neutral or weakly damped mode was unnecessary. Both approaches are based on the same observation: in non-normal systems, the resolvent and propagator operators can be made singular by perturbing them slightly, therefore the small distance to singularity can be used as a multiple-scale expansion parameter. The resulting amplitude equations have been compared with fully nonlinear simulations, both in parallel and non-parallel two-dimensional flows. In all cases, they predict accurately the supercritical or subcritical nonlinear evolution of the response, and bring insight into the weakly nonlinear mechanisms that modify the gains as the amplitude of the harmonic forcing or the initial condition varies.

For future research, we believe that the proposed amplitude equations could be employed as tools in a variety of different problems. (i) For instance, the efficiency of the WNNh model in capturing a subcritical behaviour may prove useful in the search for optimal paths to chaos or turbulence. Indeed, (2.16) could be included as a constraint in a Lagrangian optimisation problem, whose stationary point would constitute a weakly nonlinear optimal. Such an approach could complement fully nonlinear optimisations, proposed for instance in Pringle & Kerswell (2010), by providing physical understanding at a numerical cost close to the linear one. (ii) Amplitude equations could also be exploited for fully three-dimensional flows, where we expect them to still be valid since the hypothesis of two dimensionality has never been made in the developments. Again in their quality of reduced-order models, they would be all the more relevant here because assessing the three-dimensional finite-amplitude flow behaviour from DNS is generally costly. (iii) For the transient growth aspect, the assumption of a time-independent state operator and the associated operator exponential formalism are unnecessary, and we believe that the model can be applied to time-varying base flows.

Furthermore, the method presents numerous possibilities for extension, in addition to higher-order corrections. For instance, the inclusion of multiple forcing structures or trajectories: the nonlinear interaction of multiple harmonic forcings or initial conditions is particularly relevant when distinct structures lead to comparable gains, for instance

947 A43-26

optimal and sub-optimal initial conditions (Butler & Farrell 1992; Blackburn *et al.* 2008), or perturbations of different spatial wavenumbers as in jet flows forced with different azimuthal wavenumbers (Garnaud *et al.* 2013*b*). The ensuing system of coupled amplitude equations may bear a rich dynamics, such as hysteresis and chaos. Amplitude equations are useful for flow control and optimisation, as shown for instance in Sipp (2012) in the classical context of a marginally stable flow, displaying little non-normality, with a well isolated eigenvalue and a sufficiently large spectral gap. Our current efforts also involve deriving an amplitude equation for the response to stochastic forcing, as investigated in Farrell & Ioannou (1993) and Mantic-Lugo & Gallaire (2016*a*) with linear and self-consistent models, respectively.

Finally, it should be noted that the proposed method is not restricted to the Navier–Stokes equations, but applies to all nonlinear systems whose linearised operator exhibits strong non-normality (see Trefethen & Embree (2005, §§ 55–60) for a comprehensive discussion, as well as the situations discussed in the introduction). For instance in ecological models describing the temporal evolution of a population, such as the canonical Lotka–Volterra predator–prey equations, the so-called resilience of a community (spectral abscissa of the Jacobian of the system) is known to be sometimes a misleading or incomplete measure (Neubert & Caswell 1997). The conjunction of non-normality and nonlinearity is then key to predicting population extinction/survival.

Declaration of interests. The authors report no conflict of interest.

Author ORCIDs.

🔘 Yves-Marie Ducimetière https://orcid.org/0000-0003-4018-5751;

🔘 Edouard Boujo https://orcid.org/0000-0002-4448-6140;

🔘 François Gallaire https://orcid.org/0000-0002-3029-1457.

Appendix A. Harmonic gain sensitivity and comparison with the WNNh model

Let $G_o = 1/\epsilon_o$ designate the linear harmonic gain. Then $R^\dagger R \hat{f}_o = G_o^2 \hat{f}_o$ holds by definition, and implies $G_o^2 = \langle R^\dagger R \hat{f}_o, \hat{f}_o \rangle$ thanks to the chosen normalisation $\|\hat{f}_o\| = 1$. We are interested in the squared gain variation δG_o^2 (where this notation does not designate the square of the gain variation) induced by a small perturbation δL of the state operator. The latter results in the following perturbation δR of the resolvent:

$$
\begin{aligned}
\delta R &= (i\omega I - L - (\delta L))^{-1} - (i\omega I - L)^{-1} \\
&= [(i\omega I - L)(I - R(\delta L))]^{-1} - R \\
&\approx (I + R\delta L)R - R \\
&= R(\delta L)R.
\end{aligned}
\tag{A1}
$$

The gain variation is therefore

$$
\begin{aligned}
\delta G_o^2 &= \langle \delta(R^\dagger R)\hat{f}_o, \hat{f}_o \rangle = \left\langle (\delta R)^\dagger R \hat{f}_o + R^\dagger (\delta R)\hat{f}_o, \hat{f}_o \right\rangle \\
&= \left\langle R^\dagger (\delta R)\hat{f}_o, \hat{f}_o \right\rangle + \text{c.c.}
\end{aligned}
$$

$$= \left\langle R(\delta L)R\hat{f}_o, R\hat{f}_o \right\rangle + \text{c.c.}$$

$$= \left\langle (\delta L)G_o\hat{u}_o, G_o^2\hat{f}_o \right\rangle + \text{c.c.}, \tag{A2}$$

so finally

$$\delta G_o^2 = 2G_o^3 \text{Re}\left[\left\langle (\delta L)\hat{u}_o, \hat{f}_o \right\rangle\right]. \tag{A3}$$

For instance, a base flow modification δU_e results in $(\delta L)\hat{u}_o = -(\hat{u}_o \cdot \nabla)\delta U_e - (\delta U_e \cdot \nabla)\hat{u}_o = -2C(\hat{u}_o, \delta U_e)$ yielding the same formula as in Brandt *et al.* (2011) with a different normalisation.

On the other hand, the WNNh model predicts

$$Y^3 \frac{|\mu + \nu|^2}{\epsilon_o^2 |\eta|^2} + 2Y^2 \text{Re}\left[\frac{\mu + \nu}{\epsilon_o \eta}\right] + Y = \left(\frac{F}{\epsilon_o}\right)^2, \tag{A4}$$

where $Y = |\bar{a}|^2$. We identify the weakly nonlinear harmonic gain as $G^2 = Y/F^2$, and multiply (A4) by ϵ_o^2/Y

$$Y^2 \frac{|\mu + \nu|^2}{|\eta|^2} + \frac{2Y}{G_o} \text{Re}\left[\frac{\mu + \nu}{\eta}\right] + \frac{1}{G_o^2} - \frac{1}{G^2} = 0. \tag{A5}$$

Being interested in small variations around G_o^2 (that correspond to the linear limit $Y = |\bar{a}|^2 \to 0$), we write $G^2 = G_o^2 + \delta G_o^2$ with $|\delta G_o^2/G_o^2| \ll 1$. In this manner, $1/G_o^2 - 1/G^2 = \delta G_o^2/G_o^4 +$ higher order terms, eventually leading to

$$\delta G_o^2 = -2G_o^3 \text{Re}\left[\frac{|\bar{a}|^2(\mu + \nu)}{\eta}\right] + \text{h.o.t.}. \tag{A6}$$

We recognise at leading-order equation (A3) where $(\delta L)\hat{u}_o = -|\bar{a}|^2[2C(\hat{u}_o, u_{2,0}) + 2C(\hat{u}_o^*, \hat{u}_{2,2})]$. Thus, in the small gain variation limit, the WNNh model both contains the sensitivity formula of the harmonic gain to the base flow static perturbation $|a|^2 u_{2,0}$, and embeds the effect of the second harmonic $\hat{u}_{2,2}$ as well.

Appendix B. Applying the WNN models to the Navier–Stokes equations

The incompressible Navier–Stokes equations are written, after linearising around the equilibrium velocity field U_e,

$$B\frac{\mathrm{d}q}{\mathrm{d}t} = Lq + d, \tag{B1}$$

with the state vector $q = [u, p]^\text{T}$, the forcing $d = [f, 0]^\text{T}$, the singular mass matrix

$$B = \begin{bmatrix} I & 0 \\ 0 & 0 \end{bmatrix}, \tag{B2}$$

and the linearised Navier–Stokes operator

$$L = \begin{bmatrix} -(U_e \cdot \nabla) * -(* \cdot \nabla)U_e + Re^{-1}\Delta(*) & \nabla(*) \\ \nabla \cdot (*) & 0 \end{bmatrix}. \tag{B3}$$

Several subtleties arise from the peculiarity of the pressure variable that ensures the instantaneous satisfaction of the incompressibility condition: (i) the absence of time derivative of the pressure results in a singular mass matrix, (ii) forcing terms remain restricted to the momentum equations as we choose to have no source/sink of mass and (iii) the pressure is not included in the energy norm of the response. This complicates slightly the practical computation of the gain. For the harmonic response model, the resolvent operator is generalised as $R(\mathrm{i}\omega_o) = (\mathrm{i}\omega_o B - L)^{-1}$, and the gain is measured according to

$$G^2(\mathrm{i}\omega_o) = \frac{\langle \hat{\boldsymbol{q}}, \hat{\boldsymbol{q}} \rangle_B}{\langle \hat{\boldsymbol{d}}, \hat{\boldsymbol{d}} \rangle}, \tag{B4}$$

where we used the following scalar products:

$$\left. \begin{aligned} \langle \hat{\boldsymbol{q}}_a, \hat{\boldsymbol{q}}_b \rangle_B &= \int_\Omega \left(\hat{u}_{a,x}^* \hat{u}_{b,x} + \hat{u}_{a,y}^* \hat{u}_{b,y} + \hat{u}_{a,z}^* \hat{u}_{b,z} \right) \mathrm{d}\Omega, \quad \text{and} \\ \langle \hat{\boldsymbol{q}}_a, \hat{\boldsymbol{q}}_b \rangle &= \int_\Omega \left(\hat{u}_{a,x}^* \hat{u}_{b,x} + \hat{u}_{a,y}^* \hat{u}_{b,y} + \hat{u}_{a,z}^* \hat{u}_{b,z} + \hat{p}_a^* \hat{p}_b \right) \mathrm{d}\Omega. \end{aligned} \right\} \tag{B5}$$

The B-scalar product excludes pressure, such that the pseudonorm $\langle \hat{\boldsymbol{q}}, \hat{\boldsymbol{q}} \rangle_B = \|\hat{\boldsymbol{q}}\|_B^2$ is the total kinetic energy of the response. The scalar product at the denominator includes pressure, although this will not change the norm of $\hat{\boldsymbol{d}}$, namely $\langle \hat{\boldsymbol{d}}, \hat{\boldsymbol{d}} \rangle = \|\hat{\boldsymbol{d}}\|^2$, since we have no source/sink of mass. The weakly nonlinear coefficients must be considered under these scalar products. Let $\hat{\boldsymbol{q}}_o = [\hat{\boldsymbol{u}}_o, p_o]^T$ with $\|\hat{\boldsymbol{q}}_o\|_B = 1$, $\hat{\boldsymbol{d}}_o = [\hat{\boldsymbol{f}}_o, 0]^T$ with $\|\hat{\boldsymbol{d}}_o\| = 1$, and $\hat{\boldsymbol{d}}_h = [\hat{\boldsymbol{f}}_h, 0]^T$ with $\|\hat{\boldsymbol{d}}_h\| = 1$, then

$$\left. \begin{aligned} \gamma &= \langle \hat{\boldsymbol{d}}_o, \hat{\boldsymbol{d}}_h \rangle, \quad 1/\eta = \langle \hat{\boldsymbol{d}}_o, B\hat{\boldsymbol{q}}_o \rangle = \langle \hat{\boldsymbol{d}}_o, \hat{\boldsymbol{q}}_o \rangle_B, \\ \mu/\eta &= \langle \hat{\boldsymbol{d}}_o, \hat{\boldsymbol{d}}_{3,1}^{(3)} \rangle, \quad \nu/\eta = \langle \hat{\boldsymbol{d}}_o, \hat{\boldsymbol{d}}_{3,1}^{(4)} \rangle, \end{aligned} \right\} \tag{B6}$$

where $\hat{\boldsymbol{d}}_{3,1}^{(3)} = [\hat{\boldsymbol{f}}_{3,1}^{(3)}, 0]^T$, $\hat{\boldsymbol{d}}_{3,1}^{(4)} = [\hat{\boldsymbol{f}}_{3,1}^{(4)}, 0]^T$, $\hat{\boldsymbol{f}}_{3,1}^{(3)} = 2C(\hat{\boldsymbol{u}}_o, \boldsymbol{u}_{2,0})$ and $\hat{\boldsymbol{f}}_{3,1}^{(4)} = 2C(\hat{\boldsymbol{u}}_o^*, \boldsymbol{u}_{2,2})$. The pressure field has no influence on the weakly nonlinear coefficients. For instance

$$\left. \begin{aligned} 1/\eta &= \int_\Omega \left(\hat{f}_{o,x}^* \hat{u}_{o,x} + \hat{f}_{o,y}^* \hat{u}_{o,y} + \hat{f}_{o,z}^* \hat{u}_{o,z} \right) \mathrm{d}\Omega, \quad \text{and} \\ \mu/\eta &= \int_\Omega \left(\hat{f}_{o,x}^* \hat{f}_{(3,1),x}^{(3)} + \hat{f}_{o,y}^* \hat{f}_{(3,1),y}^{(3)} + \hat{f}_{o,z}^* \hat{f}_{(3,1),z}^{(3)} \right) \mathrm{d}\Omega. \end{aligned} \right\} \tag{B7}$$

The linear and nonlinear Navier–Stokes equations are solved for (u_x, u_y, p) by means of the finite element method with Taylor–Hood (P2, P2, P1) elements, respectively, after implementation of the weak form in the software FreeFem++. The steady solutions of the Navier–Stokes equations are solved using the iterative Newton–Raphson method, and the linear operators are built thanks to a sparse solver implemented in FreeFem++. The singular-value decomposition is performed in Matlab following Garnaud *et al.* (2013*b*) directly. Finally, DNS are performed by applying a time scheme based on the characteristic–Galerkin method as described in Benitez & Bermudez (2011).

For the two-dimensional flow past a BFS presented in § 2.1, we refer to Mantic-Lugo & Gallaire (2016*b*) for the validation of the codes with existing literature and the mesh convergence, since the same codes have been used. The length of the outlet channel is chosen as $L_{out} = 50$ for $Re \leq 500$ (Mantic-Lugo & Gallaire 2016*b*), $L_{out} = 65$ for

$Re = 600$ and $L_{out} = 80$ for $Re = 700$. This ensures the convergence of the linear gain and weakly nonlinear coefficients. For the plane Poiseuille studied in § 2.2, the validation is proposed in the main text.

For the transient growth model, the linearised problem is written

$$B\frac{\mathrm{d}q}{\mathrm{d}t} = Lq \quad \text{subject to} \quad q(0) = \begin{bmatrix} u(0) \\ 0 \end{bmatrix}, \tag{B8}$$

and the gain is measured as

$$G(t_o)^2 = \frac{\langle q(t_o), q(t_o)\rangle_B}{\langle q(0), q(0)\rangle_B}, \tag{B9}$$

where the pressure component of the initial condition can be chosen as $p(0) = 0$. The orthogonality properties hold under the B-scalar product, and the weakly nonlinear coefficient $\mu_2(t)$ is written

$$\mu_2(t) = \epsilon_o \frac{\langle \tilde{q}_2(t), q_l(t)\rangle_B}{\langle q_l(t), q_l(t)\rangle_B}, \tag{B10}$$

where $q_l(t) = [l(t), p_l(t)]^{\mathrm{T}}$, and where $\tilde{q}_2 = [\tilde{u}_2(t), \tilde{p}_2(t)]^{\mathrm{T}}$ is solution of

$$B\frac{\mathrm{d}\tilde{q}_2}{\mathrm{d}t} = L\tilde{q}_2 - \begin{bmatrix} C(l, l) \\ 0 \end{bmatrix}, \quad \tilde{q}_2(0) = \mathbf{0}. \tag{B11}$$

Again, pressure does not influence the weakly nonlinear coefficient since only velocity fields are involved in the scalar product. In particular at $t = t_o$, $q_l(t_o) = [v_o, p_l(t_o)]^{\mathrm{T}}$ thus $\langle q_l(t_o), q_l(t_o)\rangle_B = 1$ by construction, and

$$\mu_2(t_o) = \epsilon_o \int_\Omega \tilde{u}_{2,x}v_{o,x} + \tilde{u}_{2,y}v_{o,y} + \tilde{u}_{2,z}v_{o,z} \, \mathrm{d}\Omega. \tag{B12}$$

The software FreeFem++ is again used to solve for the velocity and pressure by means of the finite element method with Taylor–Hood elements, (P2 for velocity and P1 for pressure). The practical computation of the gain (B9) proposed in Garnaud *et al.* (2013*a*) is followed. The application of the propagator e^{Lt} (respectively its adjoint $(\mathrm{e}^{Lt})^\dagger$) are performed by integrating in time the linearised problem (B8) (respectively the adjoint problem) with the Crank–Nicolson method. The application of the inverse propagator e^{-Lt} is never needed. For the transient growth past the BFS studied in § 3.1, our linear optimisation codes are validated upon comparison with the results of Blackburn *et al.* (2008). For $(Re, t_o) = (500, 58)$, we obtained $G(t_o)^2 = 62.8 \times 10^3$, against $G(t_o)^2 = 63.1 \times 10^3$ in Blackburn *et al.* (2008). The $\approx 0.5\,\%$ relative error could be explained by the fact that our entrance length is $L_i = 5$, against $L_i = 10$ in Blackburn *et al.* (2008). For the plane Poiseuille flow analysed in § 3.2, the validation was performed thanks to the open-source results of Schmid & Henningson (2001), obtained with a Chebyshev polynomial discretisation, and where the singular-value decomposition of the matrix exponential e^{Lt} is performed directly. For the chosen set of parameters $(Re, k_x, k_z, t_o) = (3000, 0, 2, 230)$, convergence was achieved for a squared linear gain of $G(t_o)^2 = 1761.8$, against $G(t_o)^2 = 1761.9$ in Schmid & Henningson (2001).

Appendix C. Higher-order corrections of the WNNh equation

Recall (2.11) obtained at order $\sqrt{\epsilon_o}^3$

$$\Phi\bar{\boldsymbol{u}}_{3,1} = -A|A|^2\left[2C(\hat{\boldsymbol{u}}_o, \boldsymbol{u}_{2,0}) + 2C(\hat{\boldsymbol{u}}_o^*, \hat{\boldsymbol{u}}_{2,2})\right] - \hat{\boldsymbol{u}}_o\frac{\mathrm{d}A}{\mathrm{d}T} - A\hat{\boldsymbol{f}}_o + \phi\hat{\boldsymbol{f}}_h, \qquad \text{(C1)}$$

After imposition of the Fredholm alternative, leading to (2.12) for $\mathrm{d}A/\mathrm{d}T$, the relation (C1) becomes

$$\Phi\bar{\boldsymbol{u}}_{3,1} = A|A|^2\left[-2C(\hat{\boldsymbol{u}}_o, \boldsymbol{u}_{2,0}) - 2C(\hat{\boldsymbol{u}}_o^*, \hat{\boldsymbol{u}}_{2,2}) + \zeta\hat{\boldsymbol{u}}_o\right]$$
$$+ A(-\hat{\boldsymbol{f}}_o + \eta\hat{\boldsymbol{u}}_o) + \phi(\hat{\boldsymbol{f}}_h - \eta\gamma\hat{\boldsymbol{u}}_o), \qquad \text{(C2)}$$

where $\zeta = (\mu + \nu)$. For higher-order corrections of the WNNh model, the field $\bar{\boldsymbol{u}}_{3,1}$ is needed and is solution of (C2) where the operator Φ is singular since $\hat{\boldsymbol{u}}_o \neq \boldsymbol{0}$ belongs to its kernel. Since by construction $\hat{\boldsymbol{f}}_o = \epsilon_o R(i\omega_o)^\dagger\hat{\boldsymbol{u}}_o$, it follows immediately that $\langle\text{right-hand side}, \hat{\boldsymbol{f}}_o\rangle = \epsilon_o\langle R(i\omega_o)\text{right-hand side}, \hat{\boldsymbol{u}}_o\rangle$. Thus, thanks to the (imposed) orthogonality of the right-hand side with $\hat{\boldsymbol{f}}_o$ ($\langle\text{right-hand side}, \hat{\boldsymbol{f}}_o\rangle = 0$), solving the equation replacing Φ by $(i\omega_o I - L)$ leads directly to $\bar{\boldsymbol{u}}_{3,1}$ being orthogonal to $\hat{\boldsymbol{u}}_o$. Therefore, $P\bar{\boldsymbol{u}}_{3,1} = 0$ and $(i\omega_o I - L)\bar{\boldsymbol{u}}_{3,1} = \Phi\bar{\boldsymbol{u}}_{3,1}$, which implies that the field $\bar{\boldsymbol{u}}_{3,1}$ computed with $(i\omega_o I - L)$ instead of Φ is directly the particular solution of (C2). Note that $\bar{\boldsymbol{u}}_{3,1}$ appears as a true correction to $\hat{\boldsymbol{u}}_o$ in the sense of the scalar product. This property has the striking and important consequence that the operator Φ never needs to be constructed explicitly, whatever the order of the amplitude equation. The homogeneous part of the solution of (C2) is arbitrarily proportional to $\hat{\boldsymbol{u}}_o$. It can be ignored without loss of generality (Fujimura 1991). Eventually, the term $P\bar{\boldsymbol{u}}_{j,1}e^{i\omega_o t} + \text{c.c.}$ collected at $O(\sqrt{\epsilon_o}^{j+2})$ disappears if $j \geq 2$. This is due to the nullity of $\bar{\boldsymbol{u}}_{j,1}$ for even j, and to the nullity of $P\bar{\boldsymbol{u}}_{j,1}$ for odd j. Overall, the particular solution at order $\sqrt{\epsilon_o}^3$ is written

$$\boldsymbol{u}_3(t, T) = \left(\phi\hat{\boldsymbol{u}}_{3,1}^{(a)} + A\hat{\boldsymbol{u}}_{3,1}^{(b)} + A|A|^2\hat{\boldsymbol{u}}_{3,1}^{(c)}\right)e^{i\omega_o t} + A^3 e^{3i\omega_o t}\hat{\boldsymbol{u}}_{3,3} + \text{c.c.}, \qquad \text{(C3)}$$

where

$$\left.\begin{aligned}
(i\omega_o I - L)\hat{\boldsymbol{u}}_{3,1}^{(a)} &= \hat{\boldsymbol{f}}_h - \eta\gamma\hat{\boldsymbol{u}}_o, \\
(i\omega_o I - L)\hat{\boldsymbol{u}}_{3,1}^{(b)} &= -\hat{\boldsymbol{f}}_o + \eta\hat{\boldsymbol{u}}_o, \\
(i\omega_o I - L)\hat{\boldsymbol{u}}_{3,1}^{(c)} &= -2C(\hat{\boldsymbol{u}}_o, \boldsymbol{u}_{2,0}) - 2C(\hat{\boldsymbol{u}}_o^*, \hat{\boldsymbol{u}}_{2,2}) + \zeta\hat{\boldsymbol{u}}_o \\
(3i\omega_o I - L)\hat{\boldsymbol{u}}_{3,3} &= -2C(\hat{\boldsymbol{u}}_o, \hat{\boldsymbol{u}}_{2,2}).
\end{aligned}\right\} \qquad \text{(C4)}$$

The equation at order ϵ_o^2 is assembled as

$$(\Phi\bar{\boldsymbol{u}}_{4,1}e^{i\omega_o t} + \text{c.c.}) + s_4 = -2C(\boldsymbol{u}_1, \boldsymbol{u}_3) - C(\boldsymbol{u}_2, \boldsymbol{u}_2) - \partial_T\boldsymbol{u}_2 + (P\bar{\boldsymbol{u}}_{2,1}e^{i\omega_o t} + \text{c.c.}). \tag{C5}$$

As mentioned, $P\bar{\boldsymbol{u}}_{2,1} = \boldsymbol{0}$ since $\bar{\boldsymbol{u}}_{2,1} = \boldsymbol{0}$, and the forcing terms are $-2C(\boldsymbol{u}_1, \boldsymbol{u}_3)$, $-C(\boldsymbol{u}_2, \boldsymbol{u}_2)$ and $-\partial_T\boldsymbol{u}_2$. We first develop $C(\boldsymbol{u}_1, \boldsymbol{u}_3)$ as

$$C(\boldsymbol{u}_1, \boldsymbol{u}_3) = \phi A C(\hat{\boldsymbol{u}}_o, \hat{\boldsymbol{u}}_{3,1}^{(a)*}) + |A|^2 C(\hat{\boldsymbol{u}}_o, \hat{\boldsymbol{u}}_{3,1}^{(b)*}) + |A|^4 C(\hat{\boldsymbol{u}}_o, \hat{\boldsymbol{u}}_{3,1}^{(c)*})$$
$$+ \left[\phi A C(\hat{\boldsymbol{u}}_o, \hat{\boldsymbol{u}}_{3,1}^{(a)}) + A^2 C(\hat{\boldsymbol{u}}_o, \hat{\boldsymbol{u}}_{3,1}^{(b)}) + A^2|A|^2\left[C(\hat{\boldsymbol{u}}_o, \hat{\boldsymbol{u}}_{3,1}^{(c)}) + C(\hat{\boldsymbol{u}}_o^*, \hat{\boldsymbol{u}}_{33})\right]\right]e^{2i\omega_o t}$$
$$+ A^4 e^{4i\omega_o t} C(\hat{\boldsymbol{u}}_o, \hat{\boldsymbol{u}}_{33}) + \text{c.c.}, \qquad \text{(C6)}$$

then $C(\boldsymbol{u}_2, \boldsymbol{u}_2)$ as

$$
\begin{aligned}
C(\boldsymbol{u}_2, \boldsymbol{u}_2) = {} & |A|^4[C(\hat{\boldsymbol{u}}_{2,2}, \hat{\boldsymbol{u}}_{2,2}^*) + \text{c.c.}] + |A|^4 C(\boldsymbol{u}_{2,0}, \boldsymbol{u}_{2,0}) \\
& + \left[2A^2|A|^2 e^{2i\omega_o t} C(\boldsymbol{u}_{2,0}, \hat{\boldsymbol{u}}_{2,2}) + \text{c.c.}\right] + \left[A^4 e^{4i\omega_o t} C(\hat{\boldsymbol{u}}_{2,2}, \hat{\boldsymbol{u}}_{2,2}) + \text{c.c.}\right].
\end{aligned} \tag{C7}
$$

In addition,

$$
\begin{aligned}
\partial_T |A|^2 = A^* \partial_T A + A \partial_T A^* &= A^*(\phi\eta - \eta A - \zeta A|A|^2) + A(\phi\eta^* - \eta^* A^* - \zeta^* A^*|A|^2) \\
&= \phi\eta A^* + \phi\eta^* A - (\eta + \eta^*)|A|^2 - (\zeta + \zeta^*)|A|^4,
\end{aligned} \tag{C8}
$$

and

$$
\partial_T A^2 = 2A\partial_T A = 2\phi\eta A - 2\eta A^2 - 2\zeta A^2|A|^2, \tag{C9}
$$

such that

$$
\begin{aligned}
\partial_T \boldsymbol{u}_2 &= \partial_T(|A|^2 \boldsymbol{u}_{2,0} + A^2 e^{2i\omega_o t}\hat{\boldsymbol{u}}_{2,2} + A^{*2} e^{-2i\omega_o t}\hat{\boldsymbol{u}}_{2,2}^*) \\
&= (\phi\eta^* A \boldsymbol{u}_{2,0} + \text{c.c.}) - (\zeta + \zeta^*)|A|^4 \boldsymbol{u}_{2,0} - (\eta + \eta^*)|A|^2 \boldsymbol{u}_{2,0} \\
&\quad + \left[(2\phi\eta A\hat{\boldsymbol{u}}_{2,2} - 2\eta A^2\hat{\boldsymbol{u}}_{2,2} - 2\zeta A^2|A|^2\hat{\boldsymbol{u}}_{2,2})e^{2i\omega_o t} + \text{c.c.}\right].
\end{aligned} \tag{C10}
$$

Eventually, collecting all terms leads to the following particular solution for $\boldsymbol{u}_4$:

$$
\begin{aligned}
\boldsymbol{u}_4 = {} & [\phi A\hat{\boldsymbol{u}}_{4,0}^{(a)} + \text{c.c.}] + |A|^2 \boldsymbol{u}_{4,0}^{(b)} + |A|^4 \boldsymbol{u}_{4,0}^{(c)} + \cdots \\
& \left[(\phi A\hat{\boldsymbol{u}}_{4,2}^{(a)} + A^2\hat{\boldsymbol{u}}_{4,2}^{(b)} + A^2|A|^2\hat{\boldsymbol{u}}_{4,2}^{(c)})e^{2i\omega_o t} + \text{c.c.}\right] + \left[A^4 e^{4i\omega_o t}\hat{\boldsymbol{u}}_{4,4} + \text{c.c.}\right],
\end{aligned} \tag{C11}
$$

with

$$
\left.
\begin{aligned}
& -L\hat{\boldsymbol{u}}_{4,0}^{(a)} = -\eta^* \boldsymbol{u}_{2,0} - 2C(\hat{\boldsymbol{u}}_o, \hat{\boldsymbol{u}}_{3,1}^{(a)*}), \\
& -L\boldsymbol{u}_{4,0}^{(b)} = \boldsymbol{u}_{2,0}(\eta + \eta^*) - [2C(\hat{\boldsymbol{u}}_o, \hat{\boldsymbol{u}}_{3,1}^{(b)*}) + \text{c.c.}], \\
& -L\boldsymbol{u}_{4,0}^{(c)} = \boldsymbol{u}_{2,0}(\zeta + \zeta^*) - C(\boldsymbol{u}_{2,0}, \boldsymbol{u}_{2,0}) - [C(\hat{\boldsymbol{u}}_{2,2}, \hat{\boldsymbol{u}}_{2,2}^*) + \text{c.c.}] - [2C(\hat{\boldsymbol{u}}_o, \hat{\boldsymbol{u}}_{3,1}^{(c)*}) + \text{c.c.}], \\
& (2i\omega_o I - L)\hat{\boldsymbol{u}}_{4,2}^{(a)} = -2\eta\hat{\boldsymbol{u}}_{2,2} - 2C(\hat{\boldsymbol{u}}_o, \hat{\boldsymbol{u}}_{3,1}^{(a)}), \\
& (2i\omega_o I - L)\hat{\boldsymbol{u}}_{4,2}^{(b)} = 2\eta\hat{\boldsymbol{u}}_{2,2} - 2C(\hat{\boldsymbol{u}}_o, \hat{\boldsymbol{u}}_{3,1}^{(b)}), \\
& (2i\omega_o I - L)\hat{\boldsymbol{u}}_{4,2}^{(c)} = 2\zeta\hat{\boldsymbol{u}}_{2,2} - 2C(\boldsymbol{u}_{2,0}, \hat{\boldsymbol{u}}_{2,2}) - 2C(\hat{\boldsymbol{u}}_o, \hat{\boldsymbol{u}}_{3,1}^{(c)}) - 2C(\hat{\boldsymbol{u}}_o^*, \hat{\boldsymbol{u}}_{3,3}), \\
& (4i\omega_o I - L)\hat{\boldsymbol{u}}_{4,4} = -C(\hat{\boldsymbol{u}}_{2,2}, \hat{\boldsymbol{u}}_{2,2}) - 2C(\hat{\boldsymbol{u}}_o, \hat{\boldsymbol{u}}_{3,3}).
\end{aligned}
\right\} \tag{C12}
$$

The norms of the particular solutions at successive orders ϵ_o, $\sqrt{\epsilon_o}^3$ and ϵ_o^2 are outlined in 3 for the plane Poiseuille flow at $(Re, k_x, k_z) = (3000, 1.2, 0)$ considered in §2.2 and forced at $\omega_o = 0.3810$.

Despite a large harmonic gain for $\omega = 0$ as visible in figure 7, the stationary field $\boldsymbol{u}_{2,0}$ remains of reasonable amplitude as the associated Reynolds stress forcing $C(\hat{\boldsymbol{u}}_o, \hat{\boldsymbol{u}}_o^*)$ projects poorly on the most amplified singular mode for $\omega = 0$. However, the same does not hold for the stationary fields $\hat{\boldsymbol{u}}_{4,0}^{(a,b,c)}$ at order ϵ_o^2, all of significantly large amplitudes.

947 A43-32

$\|\boldsymbol{u}_{2,0}\|$	$\|\hat{\boldsymbol{u}}_{2,2}\|$				
11.5	2.07				

$\|\hat{\boldsymbol{u}}_{3,1}^{(a)}\|$	$\|\hat{\boldsymbol{u}}_{3,1}^{(b)}\|$	$\|\hat{\boldsymbol{u}}_{3,1}^{(c)}\|$	$\|\hat{\boldsymbol{u}}_{3,3}\|$		
10.6	10.6	21.7	11.4		

$\|\hat{\boldsymbol{u}}_{4,0}^{(a)}\|$	$\|\boldsymbol{u}_{4,0}^{(b)}\|$	$\|\boldsymbol{u}_{4,0}^{(c)}\|$	$\|\hat{\boldsymbol{u}}_{4,2}^{(a)}\|$	$\|\hat{\boldsymbol{u}}_{4,2}^{(b)}\|$	$\|\hat{\boldsymbol{u}}_{4,2}^{(c)}\|$
10.5×10^4	4.2×10^4	5.3×10^4	1.6×10^2	4.0×10^2	1.6×10^2

Table 3. Norms of the particular solutions at $O(\epsilon_o)$, $O(\sqrt{\epsilon_o}^3)$ and $O(\epsilon_o^2)$ for the plane Poiseuille flow at $(Re, k_x, k_z) = (3000, 1.2, 0)$ considered in § 2.2, and forced at $\omega_o = 0.3810$.

This implies that the asymptotic hierarchy is only maintained until order $\sqrt{\epsilon_o}^3$. Indeed, if it holds that

$$\sqrt{\epsilon_o} \gg \epsilon_o(\|\boldsymbol{u}_{2,0}\|, \|\hat{\boldsymbol{u}}_{2,2}\|) \gg \sqrt{\epsilon_o}^3(\|\hat{\boldsymbol{u}}_{3,1}^{(a)}\|, \|\hat{\boldsymbol{u}}_{3,1}^{(b)}\|, \|\hat{\boldsymbol{u}}_{3,1}^{(c)}\|, \|\hat{\boldsymbol{u}}_{3,3}\|) \tag{C13}$$

such that, until order $\sqrt{\epsilon_o}^3$, each order appears as a true correction of the previous one, this does not hold for order ϵ_o^2. As $\epsilon_o^2\|\hat{\boldsymbol{u}}_{4,0}^{(a)}\|$ is of order unity, it cannot be considered as a correction of the order $\sqrt{\epsilon_o}^3$ but appears directly at the base flow level, which is asymptotically ill posed.

Appendix D. Modal amplitude equation for harmonic forcing

The dominant eigenmode $\hat{\boldsymbol{q}}_1$ satisfies $L\hat{\boldsymbol{q}}_1 = \sigma_1\hat{\boldsymbol{q}}_1$. Let its small damping rate $\sigma_{1,r}$ (i.e. the real part of σ_1), be scaled in terms of ϵ_o as $\sigma_{1,r} = \theta\epsilon_o$, where $\theta = O(1)$ (and $\theta \leq 0$). The forcing frequency ω_o is detuned around the natural one, i.e. $\omega_o = \omega_1 + \beta\epsilon_o$ where ω_1 is the imaginary part of σ_1 and $\beta = O(1)$. The shift-operator procedure introduced in Meliga, Chomaz & Sipp (2009); Meliga, Gallaire & Chomaz (2012) is adopted thereafter, in order to apply the classical weakly nonlinear formalism. Namely, we perturb L as $L = \bar{L} + \epsilon_o S$ where S satisfies $S\hat{\boldsymbol{q}}_1 = \theta\hat{\boldsymbol{q}}_1$ and is such that all the other eigenvectors of L constitute its kernel (i.e. $S\hat{\boldsymbol{q}}_i = \boldsymbol{0}$ for $i = 2, 3, \ldots$). In this way, the perturbed operator $\bar{L}$ possesses the same eigenvector as L, only the eigenvalue σ_1 associated with $\hat{\boldsymbol{q}}_1$ is shifted of $-\sigma_{1,r}$ such as to be truly neutral: $\bar{L}\hat{\boldsymbol{q}}_1 = (L - \epsilon_o S)\hat{\boldsymbol{q}}_1 = L\hat{\boldsymbol{q}}_1 - \sigma_{1,r}\hat{\boldsymbol{q}}_1 = i\omega_1\hat{\boldsymbol{q}}_1$. The asymptotic multiple-scale expansion of the forced Navier–Stokes equations is expressed

$$\sqrt{\epsilon_o}\left[(\partial_t - \bar{L})\boldsymbol{u}_1\right] + \epsilon_o\left[(\partial_t - \bar{L})\boldsymbol{u}_2 + C(\boldsymbol{u}_1, \boldsymbol{u}_1)\right] + \cdots$$
$$+ \sqrt{\epsilon_o}^3\left[(\partial_t - \bar{L})\boldsymbol{u}_3 + 2C(\boldsymbol{u}_1, \boldsymbol{u}_2) + \partial_T\boldsymbol{u}_1 - S\boldsymbol{u}_1\right] + O(\epsilon_o^2) = \phi\sqrt{\epsilon_o}^3 e^{i\omega_o t}\hat{\boldsymbol{f}}_o + \text{c.c.}. \tag{D1}$$

The equation at order $\sqrt{\epsilon_o}$ reads

$$(\partial_t - \bar{L})\boldsymbol{u}_1 = 0, \tag{D2}$$

which leads to the solution $\boldsymbol{u}_1 = A(T)\hat{\boldsymbol{q}}_1 e^{i\omega_1 t} + \text{c.c.}$ At order ϵ_o, we obtain for $\boldsymbol{u}_2$ the equation

$$(\partial_t - \bar{L})\boldsymbol{u}_2 = -C(\boldsymbol{u}_1, \boldsymbol{u}_1)$$
$$= -2|A|^2 C(\hat{\boldsymbol{q}}_1, \hat{\boldsymbol{q}}_1^*) - \left[A^2 C(\hat{\boldsymbol{q}}_1, \hat{\boldsymbol{q}}_1) e^{i2\omega_1 t} + \text{c.c.}\right], \tag{D3}$$

947 A43-33

whose solution is $u_2 = |A|^2 q_{2,0} + [A^2 e^{2i\omega_o t} \hat{q}_{2,2} + \text{c.c.}]$, where

$$
\left.\begin{aligned}
-\bar{L}q_{2,0} &= -2C(\hat{q}_1, \hat{q}_1^*), \\
(2i\omega_o I - \bar{L})\hat{q}_{2,2} &= -C(\hat{q}_1, \hat{q}_1).
\end{aligned}\right\} \tag{D4}
$$

At order $\sqrt{\epsilon_o}^3$ is assembled

$$
\begin{aligned}
(\partial_t - \bar{L})u_3 &= -2C(u_1, u_2) + Su_1 - \partial_T u_1 + \phi(e^{i\beta T + i\omega_1 t}\hat{f}_o + \text{c.c.}) \\
&= \left[-2A|A|^2 \left[C(\hat{q}_{2,2}, \hat{q}_1^*) + C(q_{2,0}, \hat{q}_1) \right] + \theta A\hat{q}_1 - \hat{q}_1 \frac{\mathrm{d}A}{\mathrm{d}T} + \phi e^{i\beta T}\hat{f}_o \right] e^{i\omega_1 t} \\
&\quad + \text{c.c.} + \text{non-resonant terms},
\end{aligned} \tag{D5}
$$

where we used that $Su_1 = \theta A\hat{q}_1 e^{i\omega_1 t} + \text{c.c.}$ Cancelling the projection of the resonant part of the forcing term (inside the brackets) on the adjoint $\hat{a}_1$, results in an equation for A

$$
\frac{\mathrm{d}A}{\mathrm{d}T} = \theta A - A|A|^2 \frac{\langle 2C(\hat{q}_{2,2}, \hat{q}_1^*) + 2C(q_{2,0}, \hat{q}_1), \hat{a}_1 \rangle}{\langle \hat{q}_1, \hat{a}_1 \rangle} + \phi e^{i\beta T} \frac{\langle \hat{f}_o, \hat{a}_1 \rangle}{\langle \hat{q}_1, \hat{a}_1 \rangle}. \tag{D6}
$$

Note that, for $\omega_o = \omega_1$ (i.e. the detuning parameter $\beta = 0$), the amplitude in the linear regime, A_l, reads

$$
0 = \theta A + \phi \frac{\langle \hat{f}_o, \hat{a}_1 \rangle}{\langle \hat{q}_1, \hat{a}_1 \rangle} \Leftrightarrow A_l = -\phi \frac{\langle \hat{f}_o, \hat{a}_1 \rangle}{\langle \hat{q}_1, \hat{a}_1 \rangle} \theta^{-1}, \tag{D7}
$$

which corresponds to the following linear harmonic gain:

$$
G = \frac{\sqrt{\epsilon_o}|A_l|}{\phi\sqrt{\epsilon_o}^3} = \frac{1}{\epsilon_o} \left| \frac{\langle \hat{f}_o, \hat{a}_1 \rangle}{\langle \hat{q}_1, \hat{a}_1 \rangle} \right| \frac{\epsilon_o}{|\sigma_{1,r}|} = \left| \frac{\langle \hat{f}_o, \hat{a}_1 \rangle}{\langle \hat{q}_1, \hat{a}_1 \rangle} \right| \frac{1}{|\sigma_{1,r}|}, \tag{D8}
$$

which is different from the norm of the resolvent operator, i.e. $1/\epsilon_o$. Thus, even the matching with the linear regime is not guaranteed with this classical, modal approach.

Appendix E. Uniqueness of the operator perturbation

A sort of 'proof by contradiction' is proposed : we will perturb $R(i\omega_o)^{-1}$ with an operator of size larger than its minimum value ϵ_o and show that the subsequent amplitude equation leads to an inconsistent result.

It follows from $R(i\omega_o)^{-1}\hat{u}_o = \epsilon_o \hat{f}_o$ in (2.2) that

$$
\left[R(i\omega_o)^{-1} - \frac{\epsilon_o}{\langle \hat{g}, \hat{u}_o \rangle} \hat{f}_o \langle \hat{g}, * \rangle \right] \hat{u}_o = \mathbf{0} \tag{E1}
$$

holds for all the possible choices of $\hat{g}$ (in the main text we chose $\hat{g} = \hat{u}_o$). Without loss of generality we impose $\|\hat{g}\|^2 = 1$. Let us write $\langle \hat{g}, \hat{u}_o \rangle = |\langle \hat{g}, \hat{u}_o \rangle| e^{i\alpha}$ and define $\varepsilon \doteq \epsilon_o / |\langle \hat{g}, \hat{u}_o \rangle| \geq \epsilon_o$, which is necessarily larger than or equal to ϵ_o. We pick a $\hat{g}$ such that $\varepsilon \ll 1$, and select ε as our new small parameter. We can define the singular operator as

$$
\Phi \doteq R(i\omega_o)^{-1} - \varepsilon P, \quad \text{where } P = e^{-i\alpha}\hat{f}_o \langle \hat{g}, * \rangle \tag{E2}
$$

(implying $\|P\| = 1$). We clearly still have $\Phi\hat{u}_o = \mathbf{0}$, and we can show that $\Phi^\dagger \hat{a} = \mathbf{0}$ with $\hat{a} \doteq R(i\omega_o)^\dagger \hat{g}$ (indeed if $\hat{g} = \hat{u}_o$, we have $\hat{a} = \hat{f}_o$). We can perform the exact

947 A43-34

same asymptotic expansion as in the main text, replacing the small parameter ϵ_o by ε everywhere. In particular, the Navier–Stokes equations are forced by $\boldsymbol{F} = \sqrt{\varepsilon}^3 \hat{\boldsymbol{f}}_h \mathrm{e}^{\mathrm{i}\omega_o t} +$ c.c. The amplitude equation that we would eventually obtain is

$$\frac{1}{\eta}\frac{\mathrm{d}A}{\mathrm{d}T} = \phi\langle\hat{\boldsymbol{a}},\hat{\boldsymbol{f}}_h\rangle - |\langle\hat{\boldsymbol{g}},\hat{\boldsymbol{u}}_o\rangle|\langle\hat{\boldsymbol{a}},\hat{\boldsymbol{f}}_o\rangle A - \frac{\mu+\nu}{\eta}A\,|A|^2\,, \tag{E3}$$

with the coefficients

$$\eta = \frac{1}{\langle\hat{\boldsymbol{a}},\hat{\boldsymbol{u}}_o\rangle}, \quad \frac{\mu}{\eta} = \langle\hat{\boldsymbol{a}}, 2C(\hat{\boldsymbol{u}}_o,\boldsymbol{u}_{2,0})\rangle, \quad \frac{\nu}{\eta} = \langle\hat{\boldsymbol{a}}, 2C(\hat{\boldsymbol{u}}_o^*,\hat{\boldsymbol{u}}_{2,2})\rangle. \tag{E4a–c}$$

In the linear regime, the equilibrium solution of this amplitude equation is $A = \phi\langle\hat{\boldsymbol{a}},\hat{\boldsymbol{f}}_h\rangle/(|\langle\hat{\boldsymbol{g}},\hat{\boldsymbol{u}}_o\rangle|\langle\hat{\boldsymbol{a}},\boldsymbol{f}_o\rangle)$, which leads to a linear gain of

$$G = \frac{\|\sqrt{\varepsilon}A\hat{\boldsymbol{u}}_o\|}{\|\phi\sqrt{\varepsilon}^3\hat{\boldsymbol{f}}_h\|} = \frac{1}{\varepsilon}\frac{|\langle\hat{\boldsymbol{a}},\hat{\boldsymbol{f}}_h\rangle|}{|\langle\hat{\boldsymbol{g}},\hat{\boldsymbol{u}}_o\rangle||\langle\hat{\boldsymbol{a}},\boldsymbol{f}_o\rangle|} = \frac{1}{\epsilon_o}\frac{|\langle\hat{\boldsymbol{a}},\hat{\boldsymbol{f}}_h\rangle|}{|\langle\hat{\boldsymbol{a}},\boldsymbol{f}_o\rangle|}. \tag{E5}$$

If we force the flow with the optimal forcing structure $\hat{\boldsymbol{f}}_h = \hat{\boldsymbol{f}}_o$, we indeed recover the linear gain $G = 1/\epsilon_o$. However, the contradiction lies in the fact if we choose to force with $\hat{\boldsymbol{f}}_h = \hat{\boldsymbol{a}}$ instead, the linear gain becomes $G = (1/\epsilon_o)/|\langle\hat{\boldsymbol{a}},\boldsymbol{f}_o\rangle| \geq 1/\epsilon_o$, meaning that we found a forcing structure that led to a larger gain than $\hat{\boldsymbol{f}}_o$, which is by definition impossible. To guarantee the consistency of our amplitude equation (which must predict the correct linear gain), we must have $\hat{\boldsymbol{a}} = \hat{\boldsymbol{f}}_o$, which implies directly $\hat{\boldsymbol{g}} = \hat{\boldsymbol{u}}_o$ and $\varepsilon = \epsilon_o$. As a corollary, $\hat{\boldsymbol{a}} = \hat{\boldsymbol{f}}_o$ is also the only choice that guarantees the consistency between the amplitude equation and the sensitivity formula shown in Appendix A.

Appendix F. Higher-order corrections of the WNNt equation

Recall (3.19) obtained at order ϵ_o^2

$$\Phi\boldsymbol{u}_2 = \alpha\boldsymbol{u}_o + A^2\mathrm{e}^{-Lt}\tilde{\boldsymbol{u}}_2 - \frac{\mathrm{d}A}{\mathrm{d}T}\epsilon_o\boldsymbol{u}_o t - A\boldsymbol{u}_o. \tag{F1}$$

After satisfaction of the Fredholm alternative, which leads to an equation for the amplitude A, the relation (3.19) can be re-expressed as

$$\Phi\boldsymbol{u}_2 = A^2\left(\mathrm{e}^{-Lt}\tilde{\boldsymbol{u}}_2 - \epsilon_o\mu_2\boldsymbol{u}_o\right) \quad \text{for } t > 0, \tag{F2}$$

where the orthogonality of the right-hand side with $\boldsymbol{b}(t)$ is ensured by construction of $\mu_2(t) = \langle\tilde{\boldsymbol{u}}_2(t),\boldsymbol{l}(t)\rangle/\langle\boldsymbol{l}(t),\boldsymbol{l}(t)\rangle$ in (3.22). The general solution to (F2) reads $\boldsymbol{u}_2 = \boldsymbol{u}_2^{(\perp l)} + A_2\boldsymbol{l}(t)$. The particular solution of the system, $\boldsymbol{u}_2^{(\perp l)}$, is obtained by solving (F2) after replacing $\Phi(t)$ by e^{-Lt}. Indeed, such $\boldsymbol{u}_2^{(\perp l)}$ must be orthogonal to $\boldsymbol{l}(t)$, since $0 = \langle\text{right-hand side},\boldsymbol{b}(t)\rangle = \langle\mathrm{e}^{Lt}(\text{right-hand side}),\boldsymbol{l}(t)\rangle = \langle\boldsymbol{u}_2^{(\perp l)},\boldsymbol{l}(t)\rangle$. On the other hand, the term $A_2\boldsymbol{l}(t)$ constitutes the homogeneous part of the solution, where A_2 is a scalar amplitude. It can be kept in further calculations, provided it is included in the final amplitude for $\boldsymbol{l}(t)$, which would then become $\epsilon_o A + \epsilon_o^2 A_2 + O(\epsilon_o^3)$. Instead, and without loss of generality (Fujimura 1991), we propose to set $A_2 = 0$ such that

$$\boldsymbol{u}_2 = \boldsymbol{u}_2^{(\perp l)} = A^2\left(\tilde{\boldsymbol{u}}_2 - \mu_2\boldsymbol{l}\right) \quad \text{for } t > 0. \tag{F3}$$

In particular, this implies that the term $\partial_t(P\boldsymbol{u}_2)$ that appears at $O(\epsilon_o^3)$ actually vanishes since $P\boldsymbol{u}_2 = P\boldsymbol{u}_2^{(\perp l)} = \boldsymbol{0}$. If this is performed at each order $j \geq 3$, all the terms $\partial_t(P\boldsymbol{u}_j)$

vanish. In this way, the 'retroaction' forcing due to the operator perturbation only appears at $O(\epsilon_o^2)$.

Deriving a higher-order amplitude equation for transient growth requires introducing a very long time scale $\tau = \epsilon_o^2 t$, such that $A = A(T, \tau)$. The total derivative in T should then replaced as partial derivative, and the amplitude equation derived at order ϵ_o^2 writes $\partial_T A = A^2 \mu_2$ subject to $\lim_{t \to 0}(\alpha - A) = 0$. One gathers at order ϵ_o^3 for $t > 0$

$$
\begin{aligned}
\partial_t(\Phi u_3) &= -2A^3 e^{-Lt} C(l, u_2) - e^{-Lt} \partial_T u_2 - e^{-Lt} \partial_\tau u_1 - \partial_t(P u_2) \\
&= -2A^3 H e^{-Lt} \left[C(l, \tilde{u}_2) - \mu_2 C(l, l) \right] - 2A(\partial_T A) \left(e^{-Lt} \tilde{u}_2 - \epsilon_o \mu_2 u_o \right) - \epsilon_o u_o \partial_\tau A \\
&= -2A^3 e^{-Lt} \left[C(l, \tilde{u}_2) - \mu_2 C(l, l) + \dot{\mu}_2 (\tilde{u}_2 - \mu_2 l) \right] - \epsilon_o u_o \partial_\tau A, \quad \text{(F4)}
\end{aligned}
$$

since (i) $\partial_T u_2 = 2A(\partial_T A)(\tilde{u}_2 - \mu_2 l)$, (ii) $P u_2 = \mathbf{0}$ and (iii) $e^{-Lt} \partial_\tau u_1 = H e^{-Lt} l \partial_\tau A = H \epsilon_o u_o \partial_\tau A$. Equation (F4) is subject to $u_3(0) = \mathbf{0}$. Its particular solution yields

$$
u_3(t, T, \tau) = A(T, \tau)^3 u_3^{(a)}(t) + \frac{\partial A(T, \tau)}{\partial \tau} u_3^{(b)}(t), \quad \text{(F5)}
$$

where

$$
\left. \begin{aligned}
d_t \left[\Phi u_3^{(a)} \right] &= -2e^{-Lt} \left[C(l, \tilde{u}_2) - \mu_2 C(l, l) + \dot{\mu}_2(\tilde{u}_2 - \mu_2 l) \right], \quad \text{and} \\
d_t \left[\Phi u_3^{(b)} \right] &= -\epsilon_o u_o,
\end{aligned} \right\} \quad \text{(F6)}
$$

subject to the initial conditions $u_3^{(a)}(0) = u_3^{(b)}(0) = \mathbf{0}$. After time integration, we obtain

$$
\Phi u_3 = A^3 e^{-Lt} \tilde{u}_3 - \epsilon_o u_o t \partial_\tau A, \quad t > 0, \quad \text{(F7)}
$$

where $\tilde{u}_3$ is solution of

$$
\frac{d\tilde{u}_3}{dt} = L\tilde{u}_3 - 2 \left[C(l, \tilde{u}_2) - \mu_2 C(l, l) + \dot{\mu}_2(\tilde{u}_2 - \mu_2 l) \right], \quad \tilde{u}_3(0) = \mathbf{0}. \quad \text{(F8)}
$$

Cancelling the projection of the right-hand side of (F7) on $b(t)$, dividing the ensuing relation by $\langle b(t), u_o \rangle$ and taking the partial derivative with respect to t leads to

$$
\epsilon_o A^3 \frac{d\mu_3}{dt} = \epsilon_o \frac{\partial A}{\partial \tau}, \quad t > 0, \quad \text{(F9)}
$$

where

$$
\mu_3(t) = \epsilon_o^{-1} \frac{\langle e^{-Lt} \tilde{u}_3(t), b(t) \rangle}{\langle u_o, b(t) \rangle} = \frac{\langle \tilde{u}_3(t), l(t) \rangle}{\langle l(t), l(t) \rangle}. \quad \text{(F10)}
$$

To be meaningful, (F9) and its initial condition must be re-written solely in terms of t, which is done by evaluating $T = \epsilon_o t$ and $\tau = \epsilon_o^2 t$. The total derivative of A, denoted $d_t A$, is now needed, as it takes into account the implicit dependence of A; it reads $d_t A = \partial_t A + \epsilon_o \partial_T A + \epsilon_o^2 \partial_\tau A = \epsilon_o \partial_T A + \epsilon_o^2 \partial_\tau A$, such that

$$
\epsilon_o A^2 \frac{d\mu_2(t)}{dt} + \epsilon_o^2 A^3 \frac{d\mu_3(t)}{dt} = \frac{dA}{dt}, \quad t > 0, \quad \text{(F11)}
$$

subject to $\lim_{t \to 0}(\alpha - A(\epsilon_o t, \epsilon_o^2 t)) = 0$ so $A(t \to 0) = \alpha$ and the amplitude A is extended by continuity in $t = 0$ so as to impose $A(0) = \alpha$.

947 A43-36

Appendix G. Transient gain sensitivity and comparison with the WNNt model

We consider a linear system $\partial_t u = Lu$ subject to the initial condition $u(0)$ with $\|u(0)\| = 1$. The linear transient gain at $t = t_o$ writes $G_o = \|u(t_o)\|$. A variational method is used to derive the variation of the optimal transient gain induced by a small perturbation δL of operator. Let us introduce the Lagrangian

$$\mathcal{L} = G_o^2 - \int_0^{t_o} \left\langle \partial_t u - Lu, u^\dagger \right\rangle \mathrm{d}t - \beta \left(1 - \|u(0)\|^2 \right), \tag{G1}$$

where the Lagrange multipliers $u^\dagger$ and β enforce the constraints on the state equation and on the norm of the initial condition, respectively. Imposing $\langle \partial_u \mathcal{L}, \delta u \rangle = 0$ for all δu leads to the adjoint equation $\partial_t u^\dagger = -L^\dagger u^\dagger$, to be integrated backward in time from the terminal condition $u^\dagger(t_o) = 2u(t_o)$. Eventually, the gain variation induced by δL is

$$\delta(G_o^2) = \left\langle \frac{\partial \mathcal{L}}{\partial L}, \delta L \right\rangle = \int_0^{t_o} \left\langle (\delta L)u, u^\dagger \right\rangle \mathrm{d}t. \tag{G2}$$

(Note that formula (G2) was also derived in Meliga (2018) although using a different approach.) On the other hand, we derived in the main text for the WNNt model

$$a(t) = \frac{U_0}{\epsilon_o} \left[1 - \left(\frac{U_0}{\epsilon_o} \right)^2 2\mu_3(t) \right]^{-1/2}. \tag{G3}$$

The weakly nonlinear transient gain squared can be expressed as $G(t_o)^2 = (a(t_o)/U_0)^2$, while the linear gain squared is $G_o^2 = (1/\epsilon_o)^2$, such that

$$\frac{1}{G(t_o)^2} - \frac{1}{G_o^2} = -U_0^2 2\mu_3(t_o). \tag{G4}$$

We are interested in small variations around G_o^2, thus we write $G(t_o)^2 = G_o^2 + \delta G_o^2$ with $|\delta G_o^2/G_o^2| \ll 1$. In this manner, $1/G_o^2 - 1/G(t_o)^2 = \delta(G_o^2)/G_o^4 + \text{h.o.t.}$, eventually leading to

$$\delta(G_o^2) = 2\mu_3(t_o) \frac{U_0^2}{\epsilon_o^4}. \tag{G5}$$

In addition,

$$\mu_3(t_o) = \epsilon_o^{-1} \frac{\langle \mathrm{e}^{-Lt_o} \tilde{u}_3(t_o), b(t_o) \rangle}{\langle u_o, b(t_o) \rangle}, \tag{G6}$$

with $\tilde{u}_3(t) = -\mathrm{e}^{Lt} \int_0^t 2\mathrm{e}^{-Ls} C[\tilde{u}_2(s), l(s)] \mathrm{d}s$. Therefore

$$\begin{aligned}
\mu_3(t_o) &= -\epsilon_o^{-1} \frac{\left\langle \int_0^{t_o} 2\mathrm{e}^{-Ls} C[\tilde{u}_2(s), l(s)] \mathrm{d}s, b(t_o) \right\rangle}{\langle u_o, b(t_o) \rangle} \\
&= -\epsilon_o^{-1} \frac{\int_0^{t_o} \langle 2\mathrm{e}^{-Ls} C[\tilde{u}_2(s), l(s)], b(t_o) \rangle \mathrm{d}s}{\langle u_o, b(t_o) \rangle}. \tag{G7}
\end{aligned}$$

By definition, $b(t_o) = (\mathrm{e}^{Lt_o})^\dagger l(t_o)$ and $\langle u_o, b(t_o) \rangle = \langle \mathrm{e}^{Lt_o} u_o, l(t_o) \rangle = 1/\epsilon_o$. In addition, $(\mathrm{e}^{-Ls})^\dagger (\mathrm{e}^{Lt_o})^\dagger = (\mathrm{e}^{Lt_o} \mathrm{e}^{-Ls})^\dagger = (\mathrm{e}^{-L(s-t_o)})^\dagger$, such that

$$\mu_3(t_o) = -\int_0^{t_o} \left\langle 2C[\tilde{u}_2(s), l(s)], \left(\mathrm{e}^{-L(s-t_o)} \right)^\dagger l(t_o) \right\rangle \mathrm{d}s. \tag{G8}$$

In terms of our previous notations, we have the direct correspondence $\boldsymbol{u}(t) = \boldsymbol{l}(t)/\epsilon_o$ and $\boldsymbol{u}^\dagger(s) = (\mathrm{e}^{-L(s-t_o)})^\dagger 2\boldsymbol{u}(t_o)$, so we can write

$$\delta(G_o^2) = \left(\frac{2U_0^2}{\epsilon_o^4}\right)\left(-\frac{\epsilon_o^2}{2}\int_0^{t_o}\left\langle 2C[\tilde{\boldsymbol{u}}_2(s), \boldsymbol{u}(s)], \left(\mathrm{e}^{-L(s-t_o)}\right)^\dagger 2\boldsymbol{u}(t_o)\right\rangle \mathrm{d}s\right)$$

$$= -\int_0^{t_o}\left\langle 2C\left[(U_0/\epsilon_o)^2\tilde{\boldsymbol{u}}_2(s), \boldsymbol{u}(s)\right], \boldsymbol{u}^\dagger(s)\right\rangle \mathrm{d}s. \tag{G9}$$

The sensitivity relation (G2) is immediately recognised, where δL is here induced by the addition of $(U_0/\epsilon_o)^2\tilde{\boldsymbol{u}}_2$ to the base flow. Indeed, $U_0/\epsilon_o = a_{lin}$ is the linear solution of (G3) corresponding the limit $U_0 \to 0$, such that the flow field is described in this limit by $U(t) = U_e + a_{lin}\boldsymbol{l}(t) + a_{lin}^2\tilde{\boldsymbol{u}}_2(t) + O(\epsilon_o^3)$.

REFERENCES

ÅKERVIK, E., EHRENSTEIN, U., GALLAIRE, F. & HENNINGSON, D.S. 2008 Global two-dimensional stability measures of the flat plate boundary-layer flow. *Eur. J. Mech. B/Fluids* **27** (5), 501–513.

ASLLANI, M., LAMBIOTTE, R. & CARLETTI, T. 2018 Structure and dynamical behavior of non-normal networks. *Sci. Adv.* **4** (12), eaau9403.

BAGGETT, J.S. & TREFETHEN, L.N. 1997 Low-dimensional models of subcritical transition to turbulence. *Phys. Fluids* **9** (4), 1043–1053.

BENITEZ, M. & BERMUDEZ, A. 2011 A second order characteristics finite element scheme for natural convection problems. *J. Comput. Appl. Maths* **235** (11), 3270–3284.

BLACKBURN, H.M., BARKLEY, D. & SHERWIN, S.J. 2008 Convective instability and transient growth in flow over a backward-facing step. *J. Fluid Mech.* **603**, 271–304.

BOUJO, E. & GALLAIRE, F. 2015 Sensitivity and open-loop control of stochastic response in a noise amplifier flow: the backward-facing step. *J. Fluid Mech.* **762**, 361–392.

BRANDT, L., SIPP, D., PRALITS, J.O. & MARQUET, O. 2011 Effect of base-flow variation in noise amplifiers: the flat-plate boundary layer. *J. Fluid Mech.* **687**, 503–528.

BUTLER, K.M. & FARRELL, B.F. 1992 Three-dimensional optimal perturbations in viscous shear flow. *Phys. Fluids* A **4** (8), 1637–1650.

CHERUBINI, S., DE PALMA, P., ROBINET, J.-C. & BOTTARO, A. 2010 Rapid path to transition via nonlinear localized optimal perturbations in a boundary-layer flow. *Phys. Rev.* E **82**, 066302.

CHERUBINI, S., DE PALMA, P., ROBINET, J.-C. & BOTTARO, A. 2011 The minimal seed of turbulent transition in the boundary layer. *J. Fluid Mech.* **689**, 221–253.

CHOMAZ, J.-M. 2005 Global instabilities in spatially developing flows: non-normality and nonlinearity. *Annu. Rev. Fluid Mech.* **37** (1), 357–392.

CORBETT, P. & BOTTARO, A. 2000 Optimal perturbations for boundary layers subject to stream-wise pressure gradient. *Phys. Fluid* **12** (1), 120–130.

COSSU, C. & CHOMAZ, J.-M. 1997 Global measures of local convective instabilities. *Phys. Rev. Lett.* **78**, 4387–4390.

CRAWFORD, J.D. & KNOBLOCH, E. 1991 Symmetry and symmetry-breaking bifurcations in fluid dynamics. *Annu. Rev. Fluid Mech.* **23** (1), 341–387.

CROSS, M.C. & HOHENBERG, P.C. 1993 Pattern formation outside of equilibrium. *Rev. Mod. Phys.* **65**, 851–1112.

EHRENSTEIN, U. & GALLAIRE, F. 2005 On two-dimensional temporal modes in spatially evolving open flows: the flat-plate boundary layer. *J. Fluid Mech.* **536**, 209–218.

FARRELL, B.F. & IOANNOU, P.J. 1993 Stochastic forcing of the linearized Navier–Stokes equations. *Phys. Fluids* A **5** (11), 2600–2609.

FAUVE, S. 1998 *Pattern Forming Instabilities*, pp. 387–492. Cambridge University Press.

FUJIMURA, K. 1991 Methods of centre manifold and multiple scales in the theory of weakly nonlinear stability for fluid motions. *Proc. R. Soc. Lond.* A **434** (1892), 719–733.

GARNAUD, X., LESSHAFFT, L., SCHMID, P.J. & HUERRE, P. 2013*a* Modal and transient dynamics of jet flows. *Phys. Fluids* **25** (4), 044103.

GARNAUD, X., LESSHAFFT, L., SCHMID, P.J. & HUERRE, P. 2013*b* The preferred mode of incompressible jets: linear frequency response analysis. *J. Fluid Mech.* **716**, 189–202.

GOR'KOV, L.P. 1957 Stationary convection in a plane liquid layer near the critical heat transfer point. *Zh. Eksp. Teor. Fiz.* **6**, 311–315.

GUCKENHEIMER, J. & HOLMES, P. 1983 *Nonlinear Oscillations, Dynamical Systems, and Bifurcations of Vector Fields*. Springer.

GUSTAVSSON, L.H. 1991 Energy growth of three-dimensional disturbances in plane Poiseuille flow. *J. Fluid Mech.* **224**, 241–260.

HARAGUS, M. & IOOSS, G. 2011 *Local Bifurcations, Center Manifolds, and Normal Forms in Infinite-Dimensional Dynamical Systems*. Springer.

HOF, B., VAN DOORNE, C.W.H., WESTERWEEL, J., NIEUWSTADT, F.T.M., FAISST, H., ECKHARDT, B., WEDIN, H., KERSWELL, R.R. & WALEFFE, F. 2004 Experimental observation of nonlinear traveling waves in turbulent pipe flow. *Science* **305** (5690), 1594–1598.

JARAMILLO, J.L., MACEDO, R.P. & SHEIKH, L.A. 2021 Pseudospectrum and black hole quasinormal mode instability. *Phys. Rev.* X **11**, 031003.

KERSWELL, R.R. 2018 Nonlinear nonmodal stability theory. *Annu. Rev. Fluid Mech.* **50** (1), 319–345.

LANDAU, H.J. 1976 Loss in unstable resonators. *J. Opt. Soc. Am.* **66** (6), 525–529.

LANDAU, H.J. 1977 The notion of approximate eigenvalues applied to an integral equation of laser theory. *Q. Appl. Maths* **35** (1), 165–172.

LANDAU, L. & LIFSHITZ, E. 1987 *Fluid Mechanics*, 2nd edn. Butterworth-Heinemann.

MALKUS, W.V.R. & VERONIS, G. 1958 Finite amplitude cellular convection. *J. Fluid Mech.* **4**, 225–260.

MANNEVILLE, P. 2004 *Instabilities, Chaos and Turbulence*. Imperial College Press.

MANTIC-LUGO, V. & GALLAIRE, F. 2016*a* Saturation of the response to stochastic forcing in two-dimensional backward-facing step flow: a self-consistent approximation. *Phys. Fluids* **1** (8), 083602.

MANTIC-LUGO, V. & GALLAIRE, F. 2016*b* Self-consistent model for the saturation mechanism of the response to harmonic forcing in the backward-facing step flow. *J. Fluid Mech.* **793**, 777–797.

MELIGA, P. 2018 Linear and semi-linear analysis of large-scale oscillations in laminar and turbulent open flows. Habilitation à diriger des recherches, Aix-Marseille Université.

MELIGA, P., CHOMAZ, J.-M. & SIPP, D. 2009 Global mode interaction and pattern selection in the wake of a disk: a weakly nonlinear expansion. *J. Fluid Mech.* **633**, 159–189.

MELIGA, P., GALLAIRE, F. & CHOMAZ, J.-M. 2012 A weakly nonlinear mechanism for mode selection in swirling jets. *J. Fluid Mech.* **699**, 216–262.

MONOKROUSOS, A., ÅKERVIK, E., BRANDT, L. & HENNINGSON, D.S. 2010 Global three-dimensional optimal disturbances in the Blasius boundary-layer flow using time-steppers. *J. Fluid Mech.* **650**, 181–214.

NEUBERT, M.G. & CASWELL, H. 1997 Alternatives to resilience for measuring the responses of ecological systems to perturbations. *Ecology* **78** (3), 653–665.

ORR, W.M.F. 1907 The stability or instability of the steady motions of a perfect liquid and of a viscous liquid. Part II: a viscous liquid. *Proc. R. Irish Acad.* **27**, 69–138.

ORSZAG, S.A. 1971 Accurate solution of the Orr–Sommerfeld stability equation. *J. Fluid Mech.* **50** (4), 689–703.

PETERMANN, K. 1979 Calculated spontaneous emission factor for double-heterostructure injection lasers with gain-induced waveguiding. *IEEE J. Quant. Elect.* **15** (7), 566–570.

PRINGLE, C.C.T. & KERSWELL, R.R. 2010 Using nonlinear transient growth to construct the minimal seed for shear flow turbulence. *Phys. Rev. Lett.* **105**, 154502.

REDDY, S.C. & HENNINGSON, D.S. 1993 Energy growth in viscous channel flows. *J. Fluid Mech.* **252**, 209–238.

SCHMID, P.J. 2007 Nonmodal stability theory. *Annu. Rev. Fluid Mech.* **39** (1), 129–162.

SCHMID, P.J. & HENNINGSON, D.S. 1994 Optimal energy density growth in Hagen–Poiseuille flow. *J. Fluid Mech.* **277**, 197–225.

SCHMID, P. & HENNINGSON, D. 2001 *Stability and Transition in Shear Flows*. Springer.

SCHNEIDER, T.M., GIBSON, J.F. & BURKE, J. 2010 Snakes and ladders: localized solutions of plane Couette flow. *Phys. Rev. Lett.* **104**, 104501.

SIPP, D. 2012 Open-loop control of cavity oscillations with harmonic forcings. *J. Fluid Mech.* **708**, 439–468.

SIPP, D. & LEBEDEV, A. 2007 Global stability of base and mean flows : a general approach and its applications to cylinder and open cavity flows. *J. Fluid Mech.* **593**, 333–358.

STROGATZ, S.H. 2015 *Nonlinear Dynamics and Chaos*, 2nd edn. CRC Press.

STUART, J.T. 1958 On the nonlinear mechanics of hydrodynamic stability. *J. Fluid Mech.* **4**, 1–21.

STUART, J.T. 1960 On the nonlinear mechanics of wave disturbances in stable and unstable parallel flows. Part 1. The basic behavior in plane Poiseuille flow. *J. Fluid Mech.* **9**, 353–370.

TREFETHEN, L.N. & EMBREE, M. 2005 *Spectra and Pseudo-Spectra*. Princeton University Press.

TREFETHEN, L.N., TREFETHEN, A.E., REDDY, S.C. & DRISCOLL, T.A. 1993 Hydrodynamic stability without eigenvalues. *Science* **261** (5121), 578–584.

WALEFFE, F. 1995 Transition in shear flows, nonlinear normality versus non-normal linearity. *Phys. Fluids* **7** (12), 3060–3066.

WATSON, J. 1960 On the nonlinear mechanics of wave disturbances in stable and unstable parallel flows. Part 2. The development of a solution for plane Poiseuille and for plane Couette flow. *J. Fluid Mech.* **9**, 371–389.